University of Adelaide
Discipline of Geology & Geophysics
School of Earth and Environmental Sciences

Early Palaeozoic mafic magmatism associated with intracontinental rifting in the Harts Range, central Australia.

Christine Grace Lawley

Supervisors: John Foden & Martin Hand

November 2005

Submitted in partial fulfilment for the Honours degree of Bachelor of Science (Geology)

CONTENTS

Abstract

Mafic sills intrude the Upper Stanovos Gneiss in the southeastern Arunta Inlier, central Australia referred to here as the Stanovos Igneous Suite (SIS). The host rock Upper Stanovos Gneiss was deposited in a localised depo-centre within the Amadeus Basin at 545Ma from sediments derived from the Musgrave Block. The SIS intruded the Upper Stanovos Gneiss in a deep (approximately 16km) localised strike-slip basin (the Irindina sub-basin) formed during intracratonic rifting. LA-ICPMS U/Pb zircon dating of granites associated with the mafic rocks give 524Ma ± 8Ma. The intrusions occurred at 5.3 kbars at temperatures > 1150°C. The mafic sills are extensively boudinaged, due to the extensional Larapinta Event that occurred during the early Ordovician 480-460Ma. The event metamorphosed the Irindina sub-basin sediments and mafic volcanics to amphibolite and granulite grade.

The extent of rifting was insufficient to have enabled partial melting of the lithosphere to occur via passive rifting. This combined with coeval widespread occurrences of mafic magmatism throughout Australia, including the continental flood basalts with the same characteristic low Ba/Rb, Nb/Th and Ti/Y geochemical features as the SIS indicate the presence of a mantle plume beneath the continent during the mid to late Cambrian. The SIS has tholeiitic affinities and a N-MORB like mantle signature altered by fractional crystallisation and crustal assimilation. Two component mixing isotopic ratios indicate that the mafic rocks have a crustal influence and the granites have a mantle input. Geochemistry and isotopic signatures of the mafic rocks provide insights into the evolution of the mantle reservoir beneath a newly recognised early Palaeozoic intracratonic rift in central Australia.

Keywords: Mafic, strike slip, rifting, Arunta Inlier, mantle plume, continental flood basalts

1. Introduction

Continental rifts are the sites of sedimentary accumulation, volcanism and magmatic intrusion, with subsidence created during rifting, providing accommodation space for sediment (Wilson, 1989). Syn-rift erosion and deposition of sediment occurs as the flanks of the rift erode, with most rifts made up of a series of sub basins separated by accommodation zones (Wilson, 1989). Rifts can generate either extensional or transtensional basins. Extensional basins occur within or between plates while transtensional basins are formed when plates move in a strike-slip fashion relative to each other. Deep crustal fault structures lying adjacent to, or aiding in the creation of rift basins, may provide important conduits for magma and mineralisation en route to the surface (Dooley & McClay, 1997).

Magmas that are erupted on or emplaced below the surface in an intracontinental rift zone are predominantly derived from partial melting that occurs in the lower lithosphere and the upper asthenosphere (Ziegler, 1992). Partial melts are created when the asthenosphere upwells due to lithospheric unloading, leading to decompression of the mantle. The decrease in pressure allows the solid adiabat to cross the solidus and initiate partial melting of the asthenosphere. The thermal buoyancy of the partial melts, relative to surrounding material, enables them to rise, consequently filling the gap created by the rift (Thompson & Gibson, 1994). The volume of melt produced in an intracontinental rift zone is controlled by a number of factors including; asthenospheric mantle temperature, the resistance of the lithosphere to asthenospheric penetration and the rate of lithospheric plate movement over the source (Coffin & Eldholm, 1992).

The chemical and isotopic compositions of mafic magmas are a product of pre-emplacement magma chamber processes, which define the magma source (Amelin, 1996). These processes potentially involve contamination during magma ascent (via bulk mixing with crustal material or partial melt), lithospheric mantle assimilation accompanied by fractional crystallization, fluid exchange with the host rock during or shortly after crystallization, the depth of melting, the rate of magma transfer to the surface, the degree of melting, the existence of high-level magma storage reservoirs and the chemical and mineralogical heterogeneity of the mantle source (Amelin, 1996; Wilson, 1989). To decipher the contamination processes magma has been exposed to, the geochemical and isotopic characteristics of a standard, uncontaminated source needs to be established (Wilson, 1993). Within a rift zone setting, the source of magma can be the subcontinental lithospheric mantle (SCLM), the asthenosphere and partial melting of the lower crust (Thompson, 1994).

The southeastern Harts Range, central Australia (**Fig. 1**) provides an example of middle Cambrian rift tectonics associated with mafic magmatism. Here, mafic sills have been emplaced within Upper Stanovos Gneiss. The host gneiss (Upper Stanovos) is a correlative of the Ediacaran Arumbera Sandstone in the Amadeus Basin (545Ma Walter et al., 2000; Maidment 2005). The deposition of these units was coeval with the Petermann Orogeny (Buick et al., 2005), during which the Musgrave Block was uplifted and experienced a major episode of dextral transpression (Buick et al., 2005; Maidment et al., 2004). The Petermann Orogeny may have resulted in a continental-scale shearzone that induced dextral shearing of northern Australia, relative to the rest of Gondwanaland (Buick et al., 2005). Deposition of the protoliths of the Stanovos Gneiss occurred in a localised sub-basin within the broader Amadeus and Georgina basins (Scrimgeour & Raith, 2001) therefore forming a considerably thicker unit than

the Arumbera Sandstone (Buick et al., 2005). Rifting is the probable mechanism that enabled localized deep burial to occur and the adjacent northern margin of the Amadeus Basin provides further evidence for this, as it reflects a rift-controlled sedimentation (Flottmann et al. 2004).

The protolith sediments to the Harts Range were deposited in a deep transtensional basin referred to as the Irindina sub-basin (**Fig 2**) (Buick et al., 2005). The development of the Irindina sub-basin and emplacement of the Stanovos Igneous Suite (SIS) appears to represent part of a widespread and long-lived interval of extension throughout central Australia associated with eruptions of the Kalkarinji Continental Flood Basalts (Glass & Phillips, 2001). The Kalkarinji Continental Flood Basalts (507 ± 2Ma; Glass, 2002) represent the Antrim Plateau Volcanics (513 ± 12Ma; Hanley & Windgate, 2000) and their correlatives (**Fig 3a**).

In this contribution, further evidence is presented for large scale mafic magmatism in the Harts Range, being related to a larger continental flood basalt province (the Kalkarinji) throughout central and western Australia (Glass, 2002; Glass & Phillips 2001). It is the aim of this paper to put forward evidence in favour of the presence of a mantle plume head centred beneath central Australia in the mid to late Cambrian. Emplacement of the SIS occurred ~524±8Ma ago at high temperatures and moderate pressures after the melt had undergone fractional crystallisation and crustal contamination while being emplaced at 15-20km. The sills have undergone tectonism and metamorphism to amphibolite and granulite grade that occurred during the 480-460Ma Larapinta Event. This resulted in the sills becoming boudinaged. Relict igneous textures are however preserved, within the boudin cores.

The mantle source and petrogenesis of mafic sills are investigated in this study using geochemical and isotopic data. The study also provides data that constrains pressure, temperature and timing at which emplacement occurred to deduce burial rate during rifting and whether lithospheric thinning (measured using the stretching factor β) (**Appendix 1**) was sufficient to induce partial melting of the lithospheric mantle at normal asthenospheric temperatures. Geochronological constraints are available due to zircon bearing granitic melts crosscutting the mafic magmatism. However, variation in metamorphic grade between host rocks and the mafic sill, even though of comparable age, can also assist in timing relationships (Teale, pers. comm. 2005). The data provides an insight into the evolution of the mantle reservoir beneath a newly recognised early Palaeozoic intracontinental rift in central Australia.

2. Geological Framework

The Harts Range is located in the southeastern Arunta Inlier central Australia. The Irindina Supracrustal Assemblage (ISA) is a lithological association that forms part of the "cover" sequence in the Harts Range and was deposited during mid-late Cambrian intracratonic rifting (Buick et al., 2005). The ISA is in structural contact with an underlying Palaeoproterozoic basement complex that comprises the 1745 Ma Bruna Granitic Gneiss and the underlying 1765-1730 Ma Entia Gneiss Complex. These are located within a regional domal structure known as the Entia Dome (**Fig. 1**) (Hand et al., 1999).

Using U-Pb isotopic data (Buick et al. (2005); Maidment et al., (2004)) found that the ISA is a late Neoproterozoic to Cambrian succession, and underwent metamorphism to amphibolite and granulite grade during the Larapinta Event in the early Ordovician (Mawby et al., 1999; Maidment et al., 2004; Buick et al., 2005). The Larapinta Event occurred during a high temperature, moderate to high, pressure regime, with a peak metamorphic phase at 800°C, 10-12 kbar, and a retrograde phase at 700°C, 7 kbar (Maidment et al., 2004).

The ISA was previously included as part of the Palaeoproterozoic basement, incorporating the Entia and Bruna gneisses (Ding & James, 1988; Mawby et al. 1999). However, recent geochronological evidence obtained from detrital zircons revealed stratigraphic correlations with the surrounding Amadeus and Georgina basins (Maidment et al., 2004; Buick et al., 2005). The correlations revealed protoliths to the ISA, which were present prior to the Alice Springs Orogeny exhumation of the Arunta Inlier, were once part of the late Neoproterozoic to early Cambrian greater Centralian Superbasin (Burdett, 2004; Maidment et al., 2004; Buick et al., 2005). The precursor

basin of the ISA is referred to as the Irindina sub-basin, a deep localised strike-slip basin **(Fig. 2a)**. The Irindina sub-basin was originally situated between the present day Georgina and Amadeus basins **(Fig. 2b)**(Buick et al., 2005). The basin formed at ~550Ma during dextral shearing, which occurred in northern Australia relative to the rest of the continent (Gondwanaland at this time)(Buick et al., 2005). The Petermann Orogeny occurred coeval to the continent scale dextral shearing and induced a major episode of dextral transpression (Buick et al., 2005). The Petermann Orogeny was principally responsible for the exhumation of the Musgrave Block, which then became the initial primary sediment source for the Irindina sub-basin and Amadeus Basin depositional units (Buick et al., 2005; Maidment et al., 2004).

Excluding the basement units, the late Neoproterozoic to mid Cambrian ISA consists of six lithostratigraphic units. The Stanovos Gneiss Member is the oldest of these units, containing a lower quartz-calc-silicate and marble layer and an upper biotite-feldspar-quartz-gneiss layer of mid Neoproterozoic and early Cambrian age respectively (Hand et al., 1999). The Upper Stanovos Gneiss Member is a correlative to the Ediacaran Arumbera Sandstone of the Amadeus Basin and is overlain by the Irindina Gneiss (Walter et al., 2000). This is a unit consisting of metapelitic gneiss, metabasite and quartzofeldspathic rocks. The Irindina Gneiss is overlain by the Harts Range Meta-Igneous Complex which consists of a number of layer parallel amphibolite bodies and additionally ultramafic rocks and anorthositic gneisses (Hand et al., 1999). The geochemistry of the Harts Range Meta-Igneous Complex is indicative of rocks generated within an intracontinental rift associated with a high degree of mantle partial melting, at relatively low pressures (Lee, 2001). The Brady Gneiss is the youngest member in the Irindina Supracrustal Assemblage and overlies

the Harts Range Meta-Igneous Complex. The gneiss consists of an upper calc-silicate unit and a lower garnet-mica-bearing metapelitic unit (Hand et al., 1999).

The ISA is complexly thrust and interfolded resulting in intense layer-parallel fabrics with strong linear components (Sivell & Foden, 1985). The protolith to the ISA was a transgressive sedimentary sequence that deposited on the eroded surface of high-grade basement gneiss (i.e. the Entia Gneiss). This sedimentary sequence is shallow marine according to Struckmeyer et al., (1992).

Geological setting of the Stanovos Igneous Suite

The mafic rocks investigated here are from a newly discovered mafic sill system occurring within the ISA on the western flank of Stanovos Valley, and were emplaced within the Upper Stanovos Gneiss and are referred to here as the Stanovos Igneous Suite (SIS) (**Fig. 4**). The sills underwent metamorphism and tectonism and as a result are boudinaged with geochronological evidence indicating this deformation occurred during the Ordovician Larapinta Event (Mawby et al., 1999).

The rocks that make up the sills on the western flank of Stanovos valley in the Harts Range include amphibolite, meta-hornblende gabbro, felsic gneiss, mixed felsic/mafic rocks and plagioclase phyric dolerite with a fine grained matrix, cumulus plagioclase calcic cored, sodic rimmed phenocrysts. This make up give the dolerite a pseudo-volcanic appearance. Within the host rock there are migmatites related to the SIS. Given the mafic rocks only occur in the Upper Stanovos Gneiss and had a sheet like geometry, this indicates they were emplaced as sills.

3. Analytical Procedures

Sample Localities

Rock samples localities for 122 samples are shown in **Appendix 2**. The GPS coordinates for all samples collected are documented in **Appendix 3**.

Geochemistry

X-ray Fluorescence

Major and trace elements anlayses were conducted using 50 representative rock samples and were determined using glass discs fused with lithium meta and teraborate flux at a 1:4 ratio of sample to flux (Major) and press pellets (trace). Analyses were made using a Philips PW 1480 X-ray Fluorescence Spectrometer at the University of Adelaide. The samples were calibrated against several international and local standard reference materials.

Inductively Coupled Plasma Mass Spectrometer (ICPMS)

Rare Earth Element (REE) analyses were derived via isotope dilution mass spectrometry using the Thermo Optek Plasma Quad 3 ICP-MS by Amdel Limited, Adelaide. The sample was dissolved in solution for analysis and was fused at 1000°C with borate flux. The resultant glass was then leached with acid and diluted x10 in order to add an internal standard for instrumental drift correction.

Geochronology

Laser Ablation – (ICPMS)

Hand panning of milled samples (<500μm grain size) was done to extract zircons. Magnetic minerals were removed by hand magnet and for more precise magnetic separation using the Frantz isodynamic separator (i.e. Garnet 0.5 – 1 amperes). Final separation was prepared using heavy liquids, Acetylene Tetrabromide and for apatite/zircon separation Methylene Iodide. Zircons were then mounted using epoxy resin, polished and put into an ultrasonic bath for degassing. Zircon Ablation was completed at Adelaide Mircroscopy, University of Adelaide using the LA-ICPMS and the computer program Glitter to display ratios $^{207}Pb/^{206}Pb$, $^{235}U/^{207}Pb$, $^{238}U/^{208}Pb$ & $^{208}Pb/^{232}Th$ that were used to determine age estimates. The international standard GJ (608Ma) as well as in-house standards 91-500 (1060Ma) and BJWP (730Ma) were used to tune the instruments and calibrate the drift.

Sr-Nd-Sm Isotope Analysis

Thermal Ionisation Mass Spectrometer

Nd and Sr isotope compositions were determined using isotope dilution methods on a Finnigan MAT 262 TIMS using both static and dynamic mode, and performed at University of Adelaide. Sm isotope compositions were resolved using the Finnigan MAT 261 TIMS in static mode. Samples were spiked and run with a blank and inhouse standard. The international La Jolla standard produced $^{143}Nd/^{144}Nd$ values of 0.512117± (n=6) during the course of the study.

Mineral Chemistry

Electron Microprobe

Major-element mineral analyses were performed using a Cameca SX 51 electron microprobe at Adelaide Microscopy, University of Adelaide. These analyses were achieved via wavelength dispersive spectrometry (WDS) with a beam current of 20nA run at an accelerating voltage of 15kV. Natural and synthetic material were used as standards.

Thermobarometric Calculations

Pressure temperature calculations were done using the computer program Thermocalc v3.1 (Powell et al., 1998), the Al-in-Hornblende (Johnson & Rutherford, 1989) and the orthopyroxene-clinopyroxene magmatic thermometer (Kretz, 1982). Mineral activities were calculated using the program AX (Holland & Powell, 2000).

4. Petrography of the Stanovos Igneous Suite

(1) The mafic rocks have a primary mineral assemblage of plagioclase – orthopyroxene – clinopyroxene – olivine – ilmenite – haematite (**Fig. 5a,b,c**). The secondary metamorphic mineral assemblage contains hornblende – clinopyroxene - biotite. These coarse grained mafics could be classed as a hornblende-gabbro. The relict sub-ophitic igneous texture (**Fig. 5c**) is easily observed whereby primary orthopyroxene is within exsolution (**Fig. 5a**) and clinopyroxene is partly recrystallised. Sample CL-100 contained a quartz xenolith, which indicates crustal contamination.

(2) The finer grained mafic rocks consist of hornblende – plagioclase - ilmenite with accessory biotite – sulphide - titanite. The fine grained mafics have been recrystallised to amphibolite. Some still contain igneous minerals such as clinopyroxene. The sulphide content is typically <1%.

(3) Plagioclase phyric mafics have a volcanic nature having a fine-grained matrix with 1-6mm plagioclase phenocrysts. The mineral assemblage consists of plagioclase – hornblende – clinopyroxene – biotite - ilmenite with accessory quartz - sulphide. The rocks have been recrystallised to amphibolite.

(4) The granitic rocks are composed of quartz – plagioclase – biotite - K-spar - garnet-zircon with accessory opaques with some samples containing small amounts of hornblende. The granitic rocks are coarse grained and have a mild foliation and so have a gneissic appearance (**Fig 5d**).

(5) Typical migmatite samples contain quartz – plagioclase – biotite - garnet with accessory titanite – allanite - zircon. They contain <1% sulphides with some samples also containing minor amounts of hornblende and apatite (**Fig. 5e**).

(6) Mixed rocks (mixing has not gone to completion) are comprised of quartz – plagioclase – biotite – garnet – clinopyroxene – orthopyroxene - hornblende with accessory ilmenite and sulphide (<1%) and vermicular textures observed in plagioclase.

5. Geochemical Results

Major and Trace Element Chemistry

Major element whole rock concentrations for analysed samples from the Stanovos Igneous Suite are presented in **Table 1, 2** and **3**.

Rare Earth Element Chemistry

15 samples were analysed via isotope dilution mass spectrometry at Amdel. REE chemistry is represented in Table 4. Corresponding, REE analyses performed at Amdel and trace elements analyses performed at the University of Adelaide were plotted for comparison. These elements included Ce, Th, La & Y (Appendix 4)

Mineral Chemistry

Representative mineral analysis from rocks from the Stanovos Igneous Suite and the associated migmatite are presented in **Table 5** and **6.**

Sr-Nd-Sm Isotope Chemistry

Sm, Nd and Sr isotopic data for representative samples of the mafic, felsic and mixed rocks of the Stanovos Igneous Suite and the associated migmatite are presented in **Table 7** and **Fig 8**. The mafic rocks in the suite have $^{147}Sm/^{144}Nd$ ratios ranging from 0.1711 to 0.1841, $^{87}Sr/^{86}Sr$ ranging from 0.7061 to 0.7075 and εNd_{520Ma} values between 1.03 and 2.39.

The granitic rocks from the suite have $^{147}Sm/^{144}Nd$ ratios ranging from 0.1193 to 0.1341, $^{87}Sr/^{86}Sr$ ranging from 0.7443 to 0.7555 and εNd_{520Ma} values between –6.05 and –5.69.

The mixing rock has a $^{147}Sm/^{144}Nd$ ratio of 0.1018, $^{87}Sr/^{86}Sr$ equal to 0.7607 and an εNd_{520Ma} value of –3.40.

The migmatite has a $^{147}Sm/^{144}Nd$ ratio of 0.1360, 87Sr/86Sr equal to 0.7323 and an εNd520Ma value of –6.14.

U/Pb Zircon Dating

Zircon ages obtained from granite samples from the Stanovos Igneous Suite and the associated migmatite are presented in **Table 8** and **Fig 7**. Concordia diagrams of the combined granites have an upper intercept Pb/U age of ~ 524 ± 8Ma (**Fig. 7a**) and $^{207}Pb/^{206}Pb$ probability density data plot ages of 528Ma (**Fig. 7b**). The granites have inheritance at 550Ma. The associated migmatite had Pb/U ages of 470 ± 24Ma (**Fig. 7c**), 517 ± 21Ma (**Fig. 7d**) and inheritance occurred at 550Ma.

Pressure-Temperature Calculations

The pressure for the mafic rock was derived using Al-in-hornblende barometer by Johnson and Rutherford (1989) (**Appendix 1**). This barometer is accurate to ± 0.5kbars. This barometer was also applied to a hornblende bearing granite (Sample HR2003-14) yielding a pressure value of 5.31 ± 0.5kbars. The barometer was also applied to a hornblende bearing migmatite sample using mineral chemistry from Burdett, (2004) (Sample HR2004-4) yielding 7.7kbars.

The temperature of the mafic rock was derived using the Kretz (1982) equations, GCA 46 (opx-cpx, magmatic temperatures). These equations are based on the differences in relative Ca:Mg:Fe ratio of the minerals resulting from simultaneous transfer reaction (determines the Ca content of the mineral) and exchange reaction (determines the relative Mg:Fe2+ ratios) (Kretz, 1982). The temperature of emplacement was determined as being 1159.67 ± 44 (2σ). A visual comparison was made using the Lindsley (1983) graphical two pyroxene thermometer at the 5kbar interval (**Fig 8**). This yielded temperatures ranging from approximately 1100-1200°C.

P-T calculations for the migmatite, were performed using THERMOCALC v3.1. These calculations provided measurements of T = 660-688°C 2σ 55, P= 7.9-8.4kbars 2σ 1.2.

6. Discussion

Within the Irindina Supracrustal Assemblage of the southeastern Harts Range, central Australia, mafic intrusives occur within the Upper Stanovos Gneiss. The sedimentary protolith to the Upper Stanovos Gneiss were deposited within a strike-slip basin at 545Ma known as the Irindina sub-basin. The Irindina sub-basin formed part of the Centralian Superbasin including the adjacent Georgina and Amadeus basins. However in response to the transtensional rift setting in which the basin was initiated, deep bounding faults created voluminous accommodation space for localised deep burial. This deep burial is evident in the thickness of sedimentary units with respect to the surrounding Georgina and Amadeus correlative units.

The sediment fill for the Centralian Superbasin was derived from the exhumation of the Musgrave block during the Petermann Orogeny. By 520Ma burial depths of 16km were obtained at which point the mafic intrusives of the Stanovos Igneous Suite were emplaced at temperatures of 1150°C. The source is mildly enriched plume-like mantle and is consistent with rift evolved magmatism. The generation of mafic magmatism within a rift zone setting requires a certain amount of extension before asthenospheric upwelling will occur and induce partial melting of the lithosphere. If extension is insufficient yet magmatism still occurs, then the next step is to look at above normal mantle temperatures and how they could arise.

6.1 What do pressure/temperature/time processes say about the burial rate in the Harts Range?

Temporal Constraints on emplacement, metamorphism and tectonism of the Stanovos Igneous Suite

Laser ablation ICP-MS U-Pb zircon dating from granite veins crosscutting and intermingling with the mafic rocks constrain the minimum age of emplacement of the mafic bodies to 524±8Ma to 516±10Ma **(Fig. 7)**. This LA-ICPMS age is within error of the 520±4Ma SHRIMP dating on the same granites (Maidment, 2005). The majority of the zircons were pink/yellow/clear in colour and inclusion free, with long needle like morphology **(Fig. 9, b,e)** ranging in size from 30-60μm wide and 150-400μm long. Back scattered electron imaging revealed zoning in some of the zircons **(Fig. 9, a,c,f)**, while others had a smeared, possible metamict, appearance **(Fig. 9 d,g)**. This is likely to have occurred as a consequence of resetting during metamorphism.

If the protolith to the Upper Stanovos Gneiss was deposited at 545Ma (Maidment, 2005) and less than 25Ma later mafic intrusions associated with extensive partial melting of the sedimentary packages were introduced, then it is likely to be at moderate pressures, since large scale melting would be difficult to achieve at shallow depths and low pressures.

Burdett (2004) derived concise geobarometric calculations from interpreted magmatic assemblages in granitic rocks of the Stanovos Igneous Suite. The assumption was based on the presence of garnet bearing assemblages in granites but not in the adjacent deformed equivalent host rock. This assumption may however be incorrect and the P-T values may reflect post-sedimentary Larapinta (~450Ma) deformation and metamorphism. These calculations provided pressures of around 10kbars which if syn-basinal imply 30km of burial occurred between 545 and 520Ma

suggesting an extremely rapid burial rate of 1.3km Ma^{-1}. Burial by deposition in the absence of crustal thickening to these depths is unusual, however the analogous Petrel sub-basin of northwestern Australia located in the southern Bonaparte basin is a localised rift basin that achieved up to 25km burial through sedimentation alone. The Petrel sub-basin is considered to be an extremely deep basin, so although the 30km burial implied by Burdett (2004) for the Irindina sub-basin may be feasible, it is at the extreme of what could be achieved via sedimentary induced burial.

In the present study pressure associated with the Stanovos Event was derived using the Al-in-Hornblende barometer (Johnson & Rutherford, 1989) (**Appendix 1**) and it was applied to a syn-mafic, hornblende bearing granite (sample HR2003-14). The barometer returned a pressure of 5.3kbars, implying a less extreme, but nevertheless rapid 15.9km of burial, equivalent to a burial rate of 0.7km Ma^{-1} over the period 545-520Ma. Although the result gives a more reasonable representation and a reasonable estimate of the pressure expected (of Burdett, 2004), it was derived from one sample only. Given the opportunity for more analysis a more accurate representation of the pressures could be expected.

The results obtained in this study suggest the temperature of emplacement of the mafic intrusion was 1150°C. A visual comparison was made using the Lindsley (1983) graphical two pyroxene thermometer at the 5kbar interval (**Fig. 8a**). The temperatures observed on the visual diagram ranged from 1100-1200°C consistent with the calculated temperature.

In order to gain accurate data, clinopyroxene and orthopyroxene have to be in equilibrium and coexisting with one another. As many of the orthopyroxene-clinopyroxene pairs analysed are from pyroxene grains showing high temperature

igneous cooling histories, with coarse herring bone exsolution (**Fig 5a**) and suggestions of pigeonite inversion, it is clear that the calculated temperatures are indeed from equilibrated pairs and must represent minimum estimates of initial parental magma temperatures (**Fig 8b**).

The pressure and temperature derived for a migmatitic assemblage (sample CL-106) adjacent to the mafic sills using the average PT approaches from Powell & Holland (1994) and the software Thermocalc (Powell et al., 1998) yielded T = 660-690 degrees and P = 7.9 – 8.4 Kbar. These elevated crustal temperatures may be the result from heating of the protolith Stanovos Gneiss basin sediment-fill by the intruding mafic magmas. As a consequence these host rocks partially melted forming the migmatite (Burdett, 2004) which have temperatures of crystallisation within error of 700-750 degree granite solidus (Wilson, 1989). As the 7.9 - 8.4kbar pressure obtained is about 2.5 - 3kbars higher than that obtained through hornblende barometry on the syn-mafic granite, an additional migmatite sample was analysed (sample HR2004-4) also using the Al-in Hornblende method. This yielded a pressure of 7.7kbars, consistent with the THERMOCALC approach on these rocks. As the migmatite has a strong foliation, partly formed by the hornblende, it is most likely the hornblende equilibrium in these host rocks records recrystallisation during metamorphism. This might indicate that the maximum pressure was achieved after the mafic intrusion, perhaps during the Larapinta event at ~450 Ma. This is also consistent with prior observations that in thin-section the hornblende is zoned with high temperature tan- brown cores and greenish rims indicating amphibole grew during high temperature metamorphism and re-equilibrated at lower temperatures (Sivell et al., 1985).

Summary PT Conditions

Results indicate the mafic intrusion was emplaced as sill-like bodies at high temperatures and middle crustal pressures. The high temperatures in part can be attributed to the nature of mafic intrusions having a solidus of 1100°C. This level of heat at moderate depths is likely to melt the country rock and induce local anatexis. This in part is due to horizontal intrusions concentrating their heat at a particular level in the crust rather than dissipating their heat over a large depth as it the case with dykes (Huppert & Sparks, 1988).

6.2 Petrogenesis and Tectonic Setting of the Magmas

i. There are a number of distinct and distinguishable reasons for the variation in magmatic composition where mantle-derived magmas interact with continental crust. These include:

- Variation in the composition of the mantle source (MORB, plume or Lithospheric Mantle?) and potential mixing of mantle sources,
- Variation in the degree of partial melting of the mantle (controlled by the exhumation of the source),
- Variation in the extent of fractional crystallisation of the mantle-derived melts once they ascend into the crust (noting that fractional crystallisation will not normally occur within the mantle),
- The extent to which assimilation and contamination by continental crustal rocks occur,
- The degree of melting (anatexis) induced in the continental rocks by the mafic intrusion,
- The extent to which the composition of the magmatic rocks have been subsequently altered due metamorphism and weathering.

This section will assess these factors in order to determine the nature of the physio tectonic control on magmatism and its tectonic setting.

ii. Identification of the Mantle Source (MORB or Plume?)

This is a key issue for this study. If the Stanovos suite is MORB-like, then it implies that the basin was a passive rift and that melting was generated by adiabatic decompression of the asthenosphere. On the other hand if the mafic suite has affinities with OIB-plume related hotspot magmatism, then it suggests that the basin may have been generated by active rifting processes and that lithospheric extension need not have proceeded as much. MORB is characterised by LREE depletion, low LIL/ HREE ratios (Rb/Y = 0.3) and low U or Th/ HREE ratios (Th/Y = 0.006). Plume/ OIB type sources yield basalts with flat to slightly LREE-enriched patterns with higher LIL/HREE (Rb/Y ~ 0.7) and Th or U /HREE (Th/Y ~ 0.12). In terms of these parameters the Stanovos suite are low to moderate Ti-tholeiites and are more like plume-related (or perhaps E-MORB) basalts. They have flat to slightly LREE-enriched REE patterns (**Fig. 10**) and elevated LIL/HREE ratios. Although the latter could be due to alteration and metamorphic mobilisation, the REE are not mobile in this way. The Stanovos suite, like plume-related mantle magmas also tend to have somewhat lower $^{143}Nd/^{144}Nd$ ratios and slightly more radiogenic $^{87}Sr/^{86}Sr$ ratios than the contemporary DM (MORB) source (**Fig. 6a**) However this is also a characteristic due to crustal contamination/ assimilation (see below). OIB/plume-related magmas tend to have slightly elevated Nb/ La or Nb/K ratios by comparison with MORB. The Stanovos suite clearly has lower Nb/La or Nb/K ratios than MORB (they have slight negative Nb anomalies in the incompatible element plots Fig. 13a) and this is certainly due to the involvement of crustal assimilation. Note that as indicated in the Sr-Nd isotope plot (**Fig. 6a**) the mafic suite has probably assimilated 5-15% crust. The conclusion is that in all probability the Stanovos suite is derived from a mildly

enriched plume-like asthenospheric source that may be expected to have an elevated potential temperature.

6.3 The role of fractional crystallisation and crustal assimilation.

Fractional Crystallisation

The extent of fractional crystallisation is affected by magma rheology and the density contrast between crystals and liquid (DePaulo, 1981). The trend observed in oxide and trace element data versus Mg# imply much of the chemical variation in the Stanovos Igneous Suite may be attributed to fractional crystallisation.

The Mg-Fe ratio is particularly useful when indexing fractional crystallisation as the ratio varies in the early stages of crystallisation due to a higher Mg-Fe ratio of the liquidus ferromagnesian minerals than their host melts (Rollinson, 1993). The negative correlation of Fe_2O_3 and positive correlation of MgO with Mg# suggests that the fractionation of olivine would have been initially dominant. This is in agreement with the Harker diagram of MgO versus SiO_2 in which the negative trend implies olivine removal (**Fig. 11a**). CaO may show very slight initial increase (**Fig. 11b**), with increasing SiO_2, but is mostly depleted, suggesting the important role of clinopyroxene. Al_2O_3 also shows initial slight increase with falling Mg# or increasing SiO_2 (**Fig 11c**) indicating suggests that clinopyroxene ± olivine first crystallised without plagioclase. This is further supported by a decrease in Cr with declining Mg# (**Fig. 12**). This was then followed by Al_2O_3 depletion indicating the major role of plagioclase fractionation. These implied crystallisation controls are completely consistent with the observed mineralogy of the rocks and follow the typical low pressure phase relations of sub-alkaline basaltic melts.

These observations are analogous to fractionation trends observed by Lee (2001) in the Harts Range Dykes, Woodside Dykes and MORB (**Fig. 11**) and in the

same way the major element variation is consistent with an evolutionary path dominated by olivine fractionation and to a lesser extent clinopyroxene and plagioclase fractionation.

Assimilation and contamination by continental crustal rocks

Wallrock assimilation and fractional crystallisation are processes that can occur during ascent and emplacement of magmas resulting in modified rocks (DePaulo, 1981). These processes can be considered coupled by their heat exchange progression (DePaulo, 1981). When the elements form the structure of the crystal lattice the latent heat of crystallisation provides the heat (excess energy) required for the surrounding crust to melt allowing assimilation to occur (DePaulo, 1981). Within a rift zone setting, the source of magma can be the subcontinental lithospheric mantle (SCLM), the asthenosphere and partial melting of the lower crust (Thompson, 1994).

The degree of wallrock assimilation is dependent upon the velocity of the ascending magma (DePaulo, 1981). Rapid magma ascent will tend to minimize wallrock assimilation (DePaulo, 1981). This is likely to occur when there is minimal density contrast between the magma and the crust through which it rises (DePaulo, 1981). Basaltic (mafic) magmas have a higher density than silicic crustal rocks and would therefore ascend slowly or possibly terminate before reaching shallow crustal levels (DePaulo, 1981). A slowed magma may cool until falling below the liquidus in which case crystallisation would occur (DePaulo, 1981; Thompson, 1994). The magma may end ascent at this point unless the composition of the magma changes and reduces in density (DePaulo, 1981; Thompson, 1994; White, 1992). The amount of assimilation is dependent on a variety of the physical parameters; the temperature contrast between magma and wallrock, the rate of magma ascent, fusion temperature of wallrock and magma (DePaulo, 1981; White, 1992).

The Harker diagrams **(Fig. 11)** each show a trend of silica enrichment that directly connects the composition of the mafic magmas to the migmatites and granites. The mixed rocks lie in the middle of this trend. The isotopic composition of the mafic rocks for Nd and Sr is more mantle–like than that of the mixed magmas and granites. As illustrated in the Nd-Sr isotope diagram **(Fig. 6a)**, silica variation in the Harker diagrams is accompanied by progressive shift of isotopic composition towards the crust. As the most isotopically primitive mafic rocks are themselves already displaced crust-ward from mantle values, it is clear these have assimilated some crust and the trend continues to the granites. Interestingly the granites are still isotopically more primitive that typical crustal rocks including the Stanovos basin fill, and must be composed of a mixture of both differentiated mantle melt (~60-75%) and assimilated crust (25-40%). This is also supported by the negative Nb-anomalies. Negative Nb anomalies are characteristic of continental crust and may be an indicator of crustal involvement in contamination processes (Wilson, 1989). The mafic rocks from the SIS have negative Nb anomaly (**Fig. 10**). Another indicator of crustal contamination is high mobile Light Ion Lithophile (LIL) element and LIL cation concentrations because they are concentrated in the continental crust. The SIS mafic rocks have high concentrations in LIL cations including Rb, Ba and K and the LIL elements Pb and Sr indicating crustal contamination (**Fig.10**).

Progressive fractional crystallisation involving plagioclase and assimilation of continental crust both lead to increased negative Eu anomalies and to elevated LIL/HREE and LREE/HREE ratios that are observed as a function of increasing silica content of the suite (**Fig. 10**)

6.4 The Geochemical discrimination of tectonic setting

When using isotopic and chemical composition of rocks to deduce their petrogenesis, the effects of metamorphism also need to be taken into account. Metamorphism unless isochemical, can cause discrete modification to rock compositions thereby, preventing accurate assessment of fractionation processes occurring prior to metamorphism (Sivell et al., 1985). However incompatible elements such as Ti, Zr and Y are considered relatively immobile under most metamorphic conditions, so can be used to determine original igneous fractionation trends (Sivell et al., 1985; Rollinson, 1993).

Incompatible trace element ratio plot for mafic rocks for the Stanovos Igneous Suite from Winchester & Floyd (1977) **(Fig. 13a)** indicate subalkaline affinities. As these results are consistent with classifications derived using total alkalis vs. silica (TAS) diagram **(Fig. 13b)** of Cox et al. (1979). The mafic rocks of the Stanovos Igneous Intrusion plot in the MORB fields for both Zr-Nb-Y & MnO-TiO_2-P_2O_5 discrimination diagrams **(Fig. 14)**. Noting that the impact of crust assimilation mentioned in the previous section is to displace the mafic rock compositions from the MORB to the OIB fields, it is still reasonable to assume that the suite is a transitional MORB-OIB (plume-like) origin. They are clearly not subduction-related.

6.5 What can be deduced from mafic and felsic magma interactions?

The association of mafic and silicic magmas are known to occur in orogenic belts above subduction zones, in continental hotspots, and in regions of crustal extension (i.e. in an intracontinental rift) (Huppert and Sparks, 1988). Within these settings magmas can mix in plutons, conduits and lava flows (Snyder et al., 1997).

This process can be preserved as a homogenous rock (occurring when mixing has gone to completion) or heterogeneous rock preserving mingling structures (i.e. solidification occurs prior to completion of mixing), which have a spectrum of streaky intermingling to discrete pillows (Snyder et al., 1997). The style and dynamics of magma mingling relates to the types, sizes and shapes of mingling structures preserved (Snyder et al., 1997).

Within the Stanovos Igneous Suite there are two relationships between mafic and granitic rocks; (1) mafic rocks has been fragmented and cross cut by granitic melt **(Fig. 15 b,d & e**) and (2) heterogeneous mixing forming mingling textures **(Fig 15 f)**. Crosscutting granite relationships occur at very large scale **(Fig. 15a)** ranging from metres to kilometre scale, indicating substantial volumes of both granitic and mafic melt within the Stanovos Igneous Suite. This implies granitic melt was not a product of localised 'sweats' but were derived either from the mantle or crustal anatexis. Burdett (2004) argued that the coexisting melts indicate the mafic intrusion may have played a key role in granite generation by advecting heat into the metasedimetary pile. Furthermore Burdett (2004) claimed the unfoliated granites resemble the mineral chemistry of both the host rock (Upper Stanovos Gneiss) and the unfoliated equivalents to the Indiana wall granite on the eastern flank of Stanovos Valley (2-3km NE). The Indiana walls granite and host rock, the Upper Stanovos Gneiss have a gradational contact over 10m (Burdett, 2004). This kind of contact is indicative of local anatexis (Wolf & Wyllie, 1993).

Field relationships in which the mafic rocks have been fragmented indicate the mafic inclusions have been broken apart before the granite solidified. In other words the mafic rock crystallized out before the granite **(Fig 15)** (Wiebe, 1973). The absence of a chilled margin and the angular edges on the mafic inclusions is indicative of post

crystallization breaks (Wiebe, 1973). Ambiguities arise between fragmented and mingling rocks as large scale fragmented relationships often have small scale interfingering and scalloped boundaries, which reflect coexisting melts (**Fig 15 b**). The relationship echoes the transition of mafic melt to solid during cooling in which the hottest parts of the body are the last to have their temperature fall below the solidus and crystallise.

Granitic and Mafic Melt interactions – Two possible analogues for the Stanovos Igneous Suite: Bjerkrem-Sogndal lopolith and the Northern Santa Lucia Range

An example of large scale magma mixing occurs in the Northern Santa Lucia Range, California (Wiebe, 1969). It is thought that the large plutons of homogeneous tonalite-granodiorite within this region were produced as a result of magma mixing between quartz monzonite and gabbro magmas (Wiebe, 1969). Wiebe (1969) suggested that partial melting of metasediment was increased in the high grade region upon the emplacement of early gabbro. The resultant anatectic quartz monzonite melt then preferentially dyked the gabbro. As the quartz monzonite melt reached the interior of the gabbro, and therefore the interior of the thermal high, mixing occurred creating a tonalite-granodiorite hybrid (Wiebe, 1969). This accounts for both crosscutting felsic melts and magma mingling to produce the observed spatial and temporal relationships.

An example of commingling of magmas occurs in the Bjerkrem-Sogndal lopolith in southwest Norway (Wiebe, 1984). This intrusive body evolved by processes including crystal fractionation, multiple magma injections, mixing of varying degrees of differentiated magmas within the chamber, magma chamber enlargement (possibly involving expulsion of residual liquid), contamination from

assimilation with country rock (or silicic melts from the country rock) and commingling of contrasted magmas (Wiebe, 1984).

6.6 Need a mechanism for localised deep burial – implications for intracontinental rifting

As discerned above the Irindina Supracrustal Assemblage (ISA) of the Harts Range is situated between the present day Georgina and Amadeus basins, and was once part of the greater Centralian Superbasin (Fig. 3) (Maidment et al., 2002; Buick et al. 2005). Uplift of the Harts Range initiated at around 450Ma during the onset of the Alice Springs Orogeny (Maidment et al., 2002). This exhumation inverted the Irindina depositional basin. (Buick et al., 2005). Geochronological evidence obtained from detrital zircon populations revealed concise stratigraphic correlations between the ISA, and both the Georgina and Amadeus basins (Maidment et al., 2003). For example deposition of protolith Upper Stanovos Gneiss in the ISA was coeval with deposition of the Arumbera Sandstone in the Amadeus Basin at 545Ma (Maidment, 2005). The basins differ in thickness however, due to the Irindina sub-basin having undergone localised deep burial, whereas the proximal Amadeus and Georgina basins have relatively thin depositional units. Deep burial of Supracrustal packages can occur via compressional tectonics by inducing crustal thickening hence creating substantial topographic relief (Dooley & McClay, 1997). This increased topography provides a source for conglomerates and coarse-grained clastic units which deposit in proximal foreland basins.

Intracratonic basins can form by rifting, thermal sag or by flexture due to loading. To obtain such deep basins, normal extension is insufficient and transtension is required. Transtensional basins can have a much greater depth to width ratio. In the Irindina sub-basin, depositional sequences lack conglomerates or coarse clastics

indicating deep burial was not caused by compressional tectonics. The geometry of the 545-440Ma rifts in central Australia reflects transtensional rifting, which resulted in the formation of strike-slip basins (Fig. 2 & Fig.3) (Buick et al., 2005). The structure of strike-slip basins is characterised by steep angled faults that penetrate mid crustal levels, providing abundant accommodation space for the occurrence of thick sedimentation and rapid subsidence (Dooley & McClay, 1997; Burdett, 2004).

Sivell & Foden (1985) suggested the existence of an intracontinental rift within the Harts Range region from the presence of transitional tholeiites, and found amphibolites that are considered to be correlates of the Stanovos Igneous Suite have continental tholeiite and ocean floor basalt affinities. Furthermore, there are more alkaline affinities occurring at Mt. Ruby towards the base of the rift sequence (Sivell & Foden, 1985). This assemblage of mafic rocks is indicative of a rift environment as melts formed within a rift are temporally related to a transition from alkaline to more tholeiitic evolution (Sivell & Foden, 1985; Hopp et al., 2004).

6.7 Continent-scale Tectonic Implications

Following the breakup of Rodinia from about 725Ma (Collins & Pisarevsky, 2005), the supercontinent Gondwana assembled from the latest Neoproterozoic through to the Middle Cambrian (Glass, 2002). At this time the intraplate Petermann Orogeny, occurred in central Australia (Buick et al., 2005). The Petermann Orogeny was associated with dextral shearing of northern Australia relative to the rest of Gondwanaland coeval with large-scale north directed thrusting across the southern Amadeus foreland (Veevers, 2000). During the earliest Cambrian (550-530 Ma) the Petermann Orogeny exhumed parts of the Musgrave Block from depths of 50km.

Transtensional rifting initiated in central Australia at 545Ma, and formed deep strike-slip sub-basins creating sedimentary accumulation space for syn-orogenic detritus from the Petermann uplift (Buick et al., 2005). These sub-basins were part of greater Centralian Superbasin (Buick et al., 2005) and were located between the present day Georgina and Amadeus basins (Maidment et al., 2002). By 520Ma the strike-slip basins had accommodated 16km (=5kbar) of sediment, at which point in time mafic sills intruded the Upper Stanovos Gneiss. The emplacement of this intrusive created a major thermal event, termed the Stanovos Event and caused melting of the rift package to form coeval granites (Maidment, 2005).

During the early Cambrian, central Australia probably lay inboard of the latest Neoproterozoic to early Cambrian passive margin to the east. In the early Cambrian east Gondwanaland (Australia) had a passive margin with the proto-Pacific (Foden et al., 2005). This passive margin became a subducting margin at ~ 515Ma (Foden et al 2005).

Extension continued in central Australia until 460Ma, the period 470-440Ma is referred to as the Larapinta Event (Mawby et al., 1999) during which the Larapintine seaway linked the eastern margin of Australia to the developing Canning rift system (Fig. 16). Contractional deformation from the Alice Springs Orogeny terminated the extensional Larapinta Event at around 450Ma and exhumed the Arunta Province from beneath the Amadeus and Georgina basins. (Haines et al. 2002)

6.8 Was lithospheric thinning sufficient to induce partial melting of the asthenosphere at normal asthenospheric temperatures? Implications for a mantle plume in Central Australia.

The continental lithosphere responds to extension by crustal thinning and an increase in the geothermal gradient after rifting, which lead to syn- and post-rift basin subsidence (Kusznir et al., 1995). According to Mckenzie & Bickle, (1988) and White

et al., (1987) at normal upper asthenosphere temperatures of 1280°C if extension ceases prior to the lithosphere reducing in thickness by half, the thinned region will subside to form a sedimentary basin. The amount of extension is defined by the ratio of the final to the initial surface area 'β' **(Appendix 1)** and unless β>2 and T>1380°C very little melt is generated (Mckenzie & Bickle, 1987). Most sedimentary basins have a β<2 and are not above magmatic arcs or mantle plumes where the higher than normal asthenosphere temperatures are present (Mckenzie & Bickle, 1988). Reverse post rift modelling from present day sections may be used to constrain the beta-factor stretching estimates.

As mentioned above the Irindina sub-basin formed during early to mid Cambrian intracontinental rifting. The basin is deep and relatively narrow with respect to the bordering Georgina and Amadeus basins that are shallow and broad indicating that rifting was localised **(Fig. 2)** (Burdett, 2004). The rift system can be depicted using the magnetic map of Australia **(Fig.16)** as being approximately 70km wide, taking into account the ~100% compression the region underwent during the Alice Springs Orogeny (Dunlap et al., 1995) it can be deduced that the rift originally had a width of ~140km. To determine whether extension was sufficient in this rift to induce decompression of the mantle and subsequently melt the asthenosphere, a comparison can be can be made with the Basin and Range Province in the western U.S.A. where mantle melting does occur. This passive rift has a β=2 in which a number of localised regions β>3 (Mckenzie & Bickle, 1988). The Basin and Range has undergone a total extension of 76km in 20Ma, which equates to $3.8 km Ma^{-1}$ (Zandt et al., 1995). Given that rifting in central Australia occurred over ~ 90Ma period spanning 545Ma to 450Ma, extension was ~140km and the maximum depth of burial was achieved at ~

470Ma (Mawby et al., 1999) the extension rate can be determined. It was assumed that the basin was at its widest at this 470Ma (Nicoll et al., 1991) the extension rate would be 1.5 km Ma^{-1} assuming a constant rate of extension. From pressure calculations, it is apparent that by 520Ma ~ 55% of the maximum burial to 30km (470Ma) = maximum width in the basin had been achieved assuming a constant burial/rifting rate. Therefore at the time of intrusion at 520Ma the total extension would equate to 50km. The 50 km of extension occurring within a 25Ma period in central Australia is far less than that of the 20Ma period within the Basin and Range Province. Considering the Basin and Range Region has a β=2, the implication is that the extension within the central Australian rift is insufficient to produce large scale mantle melting without an anomalously high asthenospheric temperature. (i.e. the presence of a mantle plume).

Protoliths of the Upper Stanovos Gneiss were deposited at 545Ma. By 520Ma burial to ~ 16km had occurred at which point in time magma's were emplaced, referred to in this paper as the Stanovos Igneous Suite. This intrusion caused extensive partial melting of the country rocks. The mantle signature obtained using discrimination diagrams indicated a MORB-like source **(Fig. 14)** and therefore large degrees of mantle melting must have occurred. The mafic magmatism in the Harts Range region occurred coincident with rifting on the eastern margin of Australia i.e. the Kanmantoo rift at 524Ma (Direen & Crawford, 2003). The intrusion is also broadly coeval with the Antrim Plateau Continental Flood Basalts, Warburton Basin Volcanics, and the Table Hill Volcanics **(Fig. 3)**.

According to Glass (2002) the Antrim Plateau Continental Flood Basalts (CFB) is correlative of multiple igneous domains extending as far east as the Queensland boarder, to the Peake Piker Volcanics and as far south as the Table Hill Volcanics in

the Officer Basin **(Fig. 3a)**. Glass (2002) redefined the Antrim Plateau CFB and correlates as the Kalkarinji low-Ti CFB.

Comparisons with the SIS and the Kalkarinji low-Ti CFB using trace element ratio discrimination diagrams indicate the SIS show the characteristic low Ba/Rb, Nb/Th and Ti/Y geochemical features of the Kalkarinji low-Ti CFB (**Fig. 3).**

Although there is some scatter caused by element mobilization, the SIS show the characteristic Kalkarinji CFB geochemical signature (elevated Rb, Th, Ce - in particular) which arises from contamination of primitive basalt with North Australian continental crust (Fig. 3, Taylor, pers. Comm., 2005).

Continental flood basalt eruption periods span short time intervals in geological terms, in the order of 2-5 million years (Hanley, 2000). Since they erupt, CFB are readily eroded. The major eruptive centres are the thickest section and as a result are the last place to erode (Hanley, 2000). The amount of melt reduces if the stretching occurs over a longer period of time (i.e. 10Ma), as heat will be lost by conduction (White, 1992). Flood basalts produce vast amounts of magmatism and form in most circumstances as a consequence of a mantle plume presence beneath the continent.

The Harts Range represents the interaction between localised rifting and mantle plume generated melts. Ongoing rifting in the eastern Arunta was likely the result of thermal weakening induced by the localisation of mafic magmatism. This is also consistent with the presence of the required high T metamorphism.

Conclusions

Intracratonic rifting initiated at 545Ma in central Australia spanned 90Ma of extension. The rifting formed a deep localised strike-slip basin into which mafic magmatism was intruded at depths of 16km and temperatures of 1100ºC at 524Ma. Pressure and timing constraints on the intrusion provide a burial rate of 0.7km Ma^{-1}.

The felsic rocks within the SIS are peraluminous. The mafic rocks are tholeiitic and have MORB affinities. The rocks have been altered via fractional crystallisation and crustal assimilation.

This circumstances in which rifting and consequent mafic magmatism occurred in the Irindina sub-basin are indicative of a mantle plume presence beneath the Australian continent during mid to late Cambrian. Evidence for mafic magmatism extrusion in the presence of a mantle plume due to, the insufficient extension to form voluminous melts without above normal asthenospheric temperature, the tholeiitic N-MORB elemental signatures and the coeval widespread mafic magmatism throughout Australia including the extrusion of continental flood basalts all comply with the theory of a mantle plume presence beneath the continent at 520Ma.

Field evidence and temperature constraints indicate the granites were generated by anatexis in which the mafic sills provided the heat source.

Temporal and compositional associations of the Stanovos Igneous Suite with the Kalkarinji low-Ti flood basalts, indicate the vast magnitude of Cambrian volcanics within over a vast portion of Australia is indicative of a mantle plume.

7. References

Amelin, Y.V., Semenov, V.S., 1996. Nd and Sr isotopic geochemistry of mafic-layered intrusions in the eastern Baltic shield: implications for the evolutions of Paleoproterozoic continental mafic magmas. *Contributions to Mineralogy and Petrology*, 124, 255-272.

Bachmann, O. & Dungan, M.A., 2002. Temperature-induced Al – zoning in hornblendes of the fish Canyon magma, Colorado. *American Mineralogist*, vol. 87; p1062-1076.

Buick, I.S., Hand, M., Williams, I.S., Mawby, J., Miller, J.A. & Nicoll, R.S., 2005. Detrital zircon provenance constraints on the evolution of the Harts Range Metamorphic Complex (central Australia): links to the Centralian Superbasin. *Journal of the Geological Society of London*, vol. 162; p777-787.

Burdett, M., 2004. Melting of sequences during basin development: constraints on subsidence rates in a deep intracratonic rift system, and implications for burial mechanisms in metamorphic terrains in the Harts Range central Australia. Unpublished Honours Thesis, University of Adelaide.

Byerl,Y., Gary, R., Mrakovich, J.V. & Malcuit, R.J., 1975. Use of Fourier Shape Analysis in Zircon Petrogenetic Studies. *Geological Society of America Bulletin*, vol. 86; p 956-958.

Coffin, M.F. & Eldholm, O. 1992. Volcanism and continental break-up: a global compilation of large igneous provinces. In: Storey, B.C., Alabaster, T. & Pankhurst, F.J. (eds), 1992, *Magmatism and the Causes of Continental Break-up*, Geological Society Special Publications No. 68, pp. 17-30.

Collins, A.S. & Pisarevsky, S.A., 2005. Amalgamating eastern Gondwana: The evolution of the Circum-Indian Orogens. *Earth-Science Reviews*, vol 71; p229-270.

Crawford, A.J., Stevens, B.P.J. & Fanning, M., 1997. Geochemistry and tectonic setting of some Neoproterozoic and early Cambrian volcanics in western NSW. *Australian Journal of Earth Sciences*, vol. 44; p831-852.

DePaulo, D.J., 1981. Trace element and isotopic effects of combined wallrock assimilation and fractional crystallisation. *Earth & Planetary Science Letters*, vol. 5; p189-202.

Ding, P. & James, P.R., 1985. Structural evolution of the Harts Range area and its implications for the development of the Arunta Block, central Australia. *Precambrian Research* vol. 27, p 251-276.

Direen, N.G. & Crawford, A.J., 2003. The Tasman Line: where is it, what is it, and is it Australia's Rodinian breakup boundary? *Australian Journal of Earth Sciences*, vol. 50; p 491-502.

Dooley, T. & McClay, k., 1997. Analog modelling of pull-apart basins. AAPG Bulletin, vol. 81; p1804-1826.

Dunlap W.J., Teyssier, C., McDougell, I. & Baldwin, S., 1995. Thermal and structural evolution of the intracratonic Arltunga nappe complex, central Australia. *Tectonics*, vol. 14; 5, p1182-1204.

Flottmann, T., Hand, M., Close, D., Edgoose, C., & Scrimgeour, I., 2004. Thrust tectonic styles of the intracratonic Alice Springs and Petermann Orogenies, central Australia. *AAPG Memoir*, vol. 82, p538-557.

Glass, L.M., 2002. Petrogenesis and Geochronology of the North Australian Kalkarinji Low-Ti Continental Flood Basalt Province. PhD thesis, Australian National University, Australia.

Glass, L.M. & Phillips, D., 2001. A precise Ar-Ar age for the Kalkarinji low-Ti Continental Flood Basalt Province of northern Australia. Unpublished thesis, Australian National University.

Haines, P.W., Hand, M. and Sandiford, M., 2001. Palaeozoic synorogenic sedimentation in central and northern Australia: a review of distribution and timing with implications for the evolution of intracontinental orogens. *Australian Journal of Earth Sciences*, vol. 48; p911-928.

Hanley, L.M. & Wingate, M.T.D., 2000. SHRIMP zircon age for an early Cambrian dolerite dyke: and intrusive phase of the Antrim Plateau Volcanics of northern Australia. *Australian Journal of Earth Science*, vol. 47; p1029-1040.

Hill, M.D. & Abbott, R.N. Jr, 1989. Mingled gabbroic and granitic magmas in the Northern Bays-Of-Main Complex, Calais area. *Igneous and Metamorphic Geology*, vol. 4; p35-43.

Hopp, J., Trieloff, M. & Altherr, R., 2004. Neon isotopes in mantle rocks from the Red Sea region reveal large-scale plume-lithosphere interaction. *Earth and Planetary Science Letters*, 219, 61-76.

Huppert, H.E. & Sparks, R.S.J., 1988. The fluid dynamics of crustal melting by injection of basaltic sills. *Transactions of the Royal Society of Edinburgh: Earth Sciences*, vol. 79; p 237-243.

Johnson, M.C. & Rutherford, M.J., 1989. Experimental calibrations of the aluminium-in-hornblende geobarometer with application to the Long Valley caldera (California) volcanic rocks. *Geology*, vol. 17; p 837-841.

Kretz, R., 1982. Transfer and exchange equilibria in a portion of the pyroxene quadrilateral as deduced from natural and experimental data. *Geochimica et Cosmochimica Acta*, vol. 46; p 411-421.

Kusznir,N.J., Roberts, A.M. & Morley, C.K., 1995. Forward and reverse modelling of rift basin formation. Geological Society, London, Special Publication, vol. 80; p 33-56.

Lee, M.J., 2001. Contrasting Sources of Palaeozoic Mafic Dykes During Intracratoic Rifting in Central Australia. *Unpublished Honours Thesis, University of Adelaide.*

Lindsley, D.H., 1983. Pyroxene thermometry. *American Mineralogist* vol. 68;5-6, p 477-493.

Liu, S.R., Fleming, P.D., 1990. mafic dykes and their setting in the southern Adelaide Fold Belt, South Australia. In: Parker, A.J., Rickwood, P.C., Tucker,D.H (Eds), Mafic Dykes and Emplacement Mechanisms. A.A. Balkema Rotterdam, P401-415.

Maidment, D.W., Williams, I.S., 2003. Detrital zircon correlation of granulite-facies metasediments with low-grade sedimentary sequences, Harts Range region, central Australia. *Geological Society of America*, 2003 annual meeting, 344.

Maidment, D., Williams, I. & Hand, M., 2004. The harts Range Metamorphic Complex- an early Neoproterozoic to Cambrian metamorphosed rift sequence in the eastern Arunta Region. *Record of Abstracts – Annual Geoscience Exploration Seminar (AGES)*, p29 – 31.

Maidment, D.W., 2005. Palaeozoic high-grade metamorphism within the Centralian Superbasin, Harts Region, central Australia. PhD Thesis, Australian National University, Australia.

Manley, C.R. & Bacon, C.R., 2000. Rhyolite thermobarometry and the shallowing of the magma reservoir, Coso Volcanic Field, California. *Journal of Petrology*, vol. 41; p149-174.

Mawby, J., Hand, M. & Foden, J., 1999. Sm-Nd evidence for high-grade Ordovician metamorphism in the Arunta Block, central Australia. *Journal of Metamorphic Geology*, vol. 17, p 653-668.

Mckenzie, D. & Bickle, M.J., 1988. The Volume and Composition of Melt Generated by Extension of the Lithosphere. *Journal of Petrology*, 29, 625-679.

Miller, J. & Srogi, L.A 1999. Field evidence from the Arden Pluton (PA-DE) for interactions between mafic and silicic magmas at depth in the crust. *Abstracts with Programs – Geological Society of America*, vol. 31; 2 p57.

Nicoll, R.S., Gorter, J.D & Owen.M, 1991. Ordovician sediments in the Waterhouse Range Anticline, Amadeus Basin, central Australia: Their interpretive and tectonic implications. *Bulletin* 236 p 277-284.

Powell, C.McA., Li, Z.X., McElhinny, M.W., Meert, J.G., and Park, J.K., 1993. Paleomagnetic constraints on the timing of the Neoproterozoic breakup of Rodinia and the Cambrian formation of Gondwana, *Geology*, vol. 21; p889-892.

Powell, R., Holland, T. & Worley, B., 1998. Calculating phase diagrams involving solid solutions via non-linear equations with examples using THERMOCALC. Journal of Metamorphic Geology, vol. 16; 4, p 557-588.

Scrimgeour, I. & Raith, J., 2001. Some tectonothermal surprises in the eastern Arunta Province. *Annual Geoscience Exploration Seminar (AGES)* p 4.

Sivell, W.J. & Foden, J.D., 1985. Banded amphibolites of the Harts Range Meta-Igneous Complex, central Australia: an early Proterozoic basalt-tonalite suite. *Precambrian Research*, vol. 28; p223-252.

Sivell, W.J., Foden, J.D. & Lawrence, R.W., 1985. The Entire anorthositic gneiss, eastern Arunta Inlier, central Australia: geochemistry and petrogenesis. Australian Journal of Earth Sciences, vol. 32; p449-465.

Snyder, D., Crambles, C., Tait, S., & Wiebe, R.A., 1997. Magma mingling in dikes and sills. *Journal of Geology*, vol. 105; 1 p75-86

Stern, R.A., Fletcher, I.R., Rasmussen, B., McNaughton, N.J. & Griffin, B.J., 2005. Ion microprobe (NanoSIMS 50) Pb-isotope geochronology at < 5μm scale. *Revised Manuscript for the International Journal of Mass Spectrometry*, University of Western Australia.

Struckmeyer, H.I.M., Totterdell, J. & Rose, I.B., 1992. Australia: Evolution of a Continent. Bureau of Mineral Resources, Geology and Geophysics.

Thompson, R.N. & Gibson, S.A., 1994. Magmatic expression of lithospheric thinning across continental rifts. *Tectonophysics*, 233, 41-68.

Veevers, J.J., 2000. Billion year earth history of Australia and neighbours in Gondwanaland, GEMOC Press, Sydney.

Walter M.R., Veervers J.J., Calver C.R., Gorjan, P., & Hill, A.C., 2000. Dating the 840-544 Ma Neoproterozoic interval by isotopes of strontium, carbon, and sulphur in seawater, and some interpretative models. *Precambrian Research*, vol. 100, p371-433.

White, R.S., Spence, G.D., Fowler, S.R., McKenzie, D.P., Westbrook, G.K. & Bowen, A.N., 1987. Magmatism at rifted continental margins. *Nature*, 330, 439-444.

White, R.S., 1992. magmatism during and after continental break-up. In: Storey, B.C., Alabaster, T. & Pankhurst, F.J. (eds), 1992, Magmatism and the Causes of Continental Break-up, *Geological Society Special Publications* No.68, p. 1-16.

Wiebe, R.A., 1969. Large-scale mixing of magmas in the northern Santa Lucia Range, California. *Special Papers - Geological Society of America*, p. 319.

Wiebe, R.A., 1973. Relations between coexisting basaltic and granitic magmas in a composite dike. *American Journal of Science*, vol. 273; p130-151.

Wiebe, R.A., 1984. Commingling of magmas in the Bjerkrem-Sogndal lopolith (southwest Norway): evidence for the composition of residual liquids. *Lithos*, vol. 17; p171-188.

Wilson, M., 1989. Igneous Petrogenesis: A global tectonic approach. London, Unwin hyman pp 325-374.

Wilson, M., 1993. Geochemical signatures of oceanic and continental basalts: a key to mantel dynamics? *Journal for the Geological Society of London*, Vol 150, pp. 977-990.

Winchester, J.A. & Floyd, P.A., 1997. Geochemical discrimination of different magma series and their differentiation products using immobile elements. *Chemical Geology*, Vol 20;4, p 325-343.

Wolf, M.B. & Wyllie, P.J., 1993. Garnet growth during amphibolite anatexis: implications of a garnetiferous restite. Journal of Geology, vol. 101, p 357-373.

Zandt, G., Meyers, S.C. & Wallace, T.C., 1995. Crust and mantle structure across the Basin and Range–Colorado Plateau boundary at 37°N latitude and implications for Cenozoic extensional mechanism. Journal of Geophysical Research, vol. 100; p10529-10548.

Zhao, J.X., 1992. Proterozoic crust-mantle evolution in central Australia: Geochemical and isotopic constraints. PhD Thesis, University of Adelaide.

Ziegler, P.A., 1992. Plate tectonics, plate moving mechanisms and rifting. *Tectonophysics*, 215, 9-3

Acknowledgements

I would like to thank my supervisors Associate Professor Martin Hand and Professor John Foden for their academic support throughout the year. Your guidance this year has been greatly appreciated. Stacey Curtis for being a wonderful friend and colleague. I enjoyed your company in the field immensely and I appreciate all the numerous times you've helped me with my work this year. Mark Burdett for giving up your time to assist in fieldwork. It was a great trip and I have loads of great memories.
I would also like to extend my thanks to the CERG boys, especially Matt Gray, Justin Payne and Ben Wade for all their hours spent showing me how to run programs etc. Thankyou to Angus Netting and John Terlet from Adelaide Microscopy. Their excellent interpersonal skills made learning to run complex equipment far less daunting. Thankyou to John Stanley, David Bruce, David Ladd and Joanne Manuel for all your help this year. I know you put a lot of work into the school so finding time for demanding honours students is commendable.
I would also like to thank Pierre-alain Wülser for his help in zircon separation, your definitely a pro! A big thankyou is also extended to Ben Goskin and Chris Field from the NTGS for lending us essential field equipment and providing a storage area for our vast quantity of rocks.
The honours crew have been sensational this year. Stacey as affomentioned was incredibly helpful and funny. Sarah who's always there for a chat, laugh, drink, camping trip or all four rolled into one. Thankyou for Jess for keeping me well fed on taste sensations from her bakery and for lots of great chats. Also for all the support you've given not only to me but other honours students too. Thankyou to Cat for providing endless distractions, which were of course to prevent your colleagues from having a meltdown. Seriously though I've enjoyed your company this year because you are a very bubbly person who tells it like it is. Speaking of telling it like it is thankyou to Diana. You were the one who stopped me from dropping out earlier in the year and I'm so glad you did. I like your honesty and ability to express your feelings as well as your sense of humour. Thankyou DC for keeping me company through the entire process of geochronology. Your Red Dwarf quoting is impeccable and I find you very funny when you complain. I would also like to extend my thanks to Anna for being our tour guide in Tasmania, also thanks for the homegrown apples and the cheese. Thankyou Rachel for all the wonderful chats, especially about netball. I appreciate proof reading done by David McAvaney our pseudo-honours student. Thankyou Stef and Henry, I hope your studies next year go really well.
A big thankyou goes to Graham and Ro Teale for your support and encouragement this year, it has been fantastic.
Last but not least thankyou Jim. You kept my head above water and did everything in your power to help lighten the burden of honours. I'm sure you felt as if you were going through it a second time and felt all my stress and worries as if they were your own. Thankyou for making my dinner every night for weeks, lending me your car so I didn't have to walk home late at night and giving me hugs when I just wanted to cry. Honey you are a rock!

This project was completed through the Continental Evolution Research Group (CERG), who has provided financial support for this project.

Figures

Tables

Appendices

Figure 1

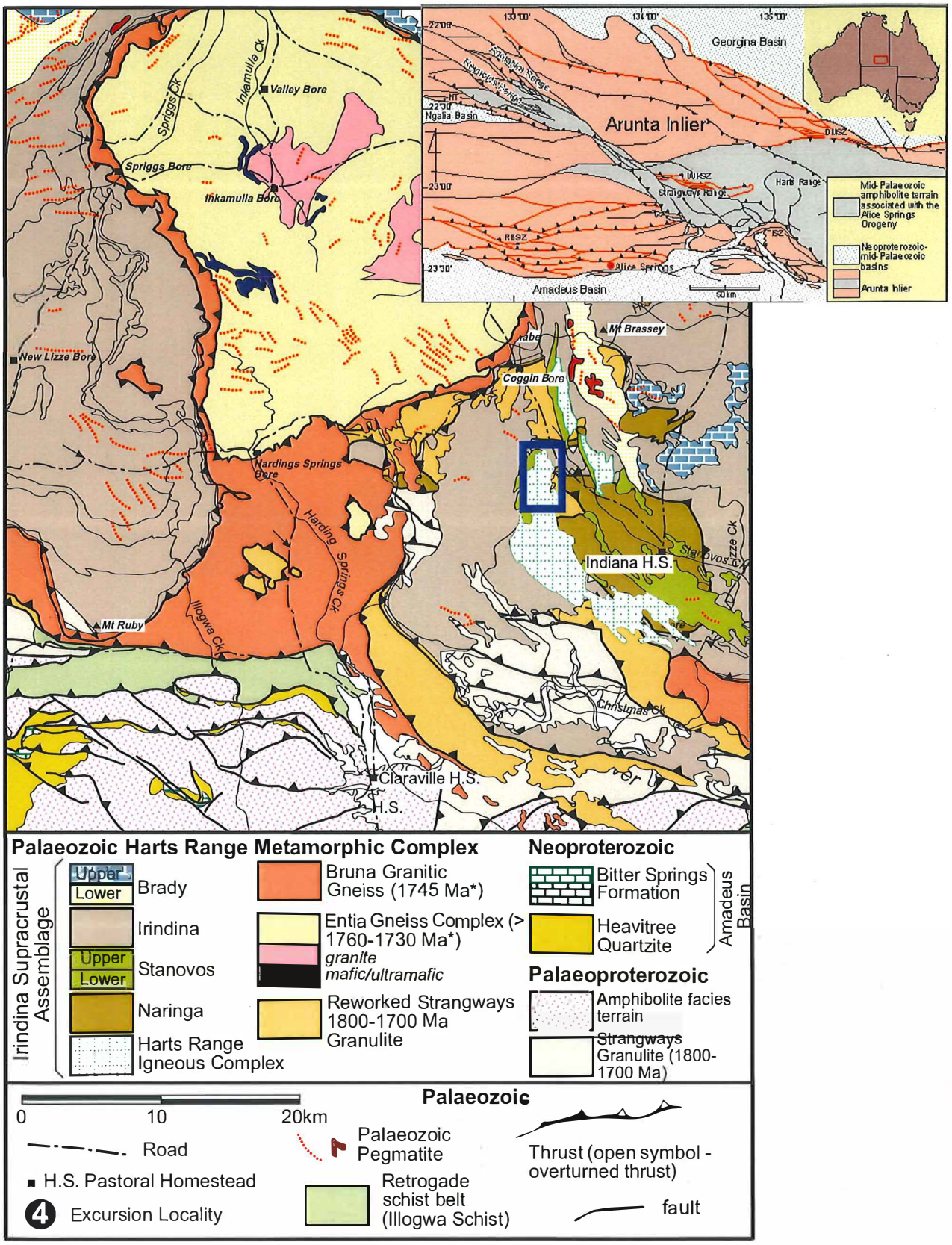

Figure 1: Geological map of the Harts Range, southeastern Arunta Block, showing structural relationships between the Palaeoproterozoic Strangways Metamorphic Complex and the Entia Gneiss Complex, with the early Cambrian Irindina Supracrustal Assemblage. The blue rectangle approximately 5km south of Coggin Bore marks the position of figure 4.

Figure 2

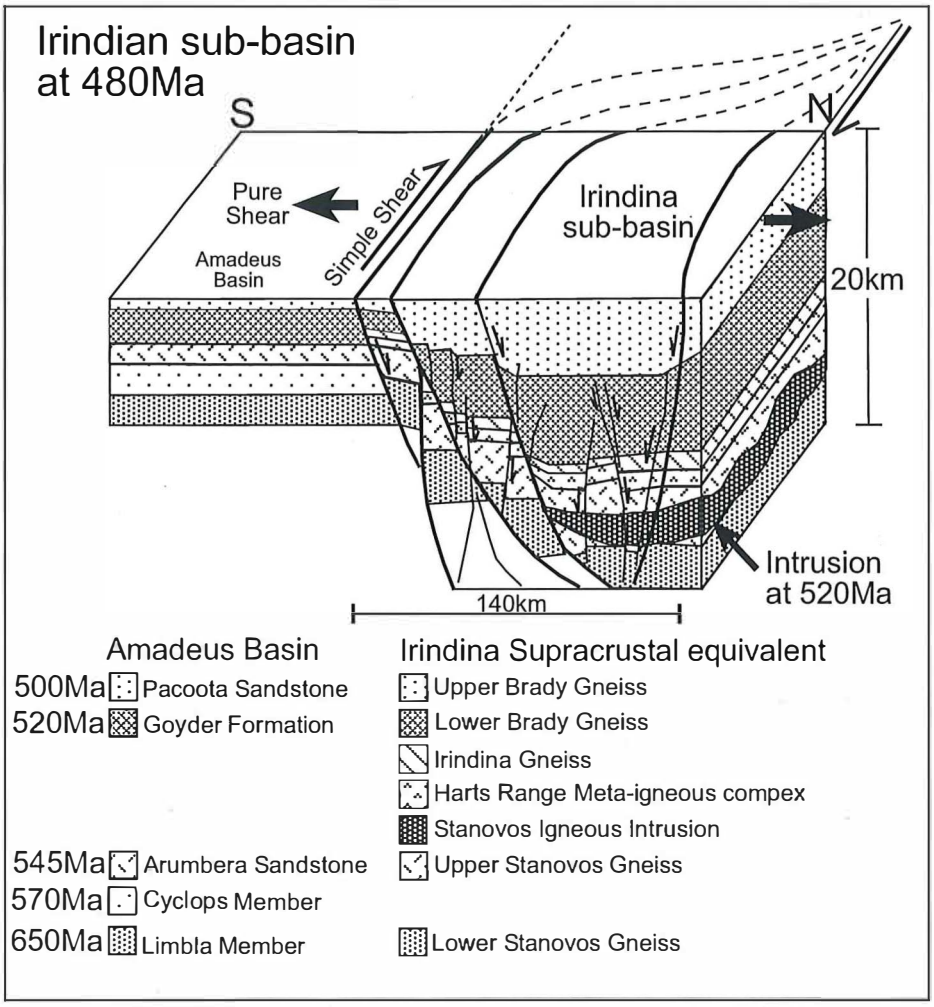

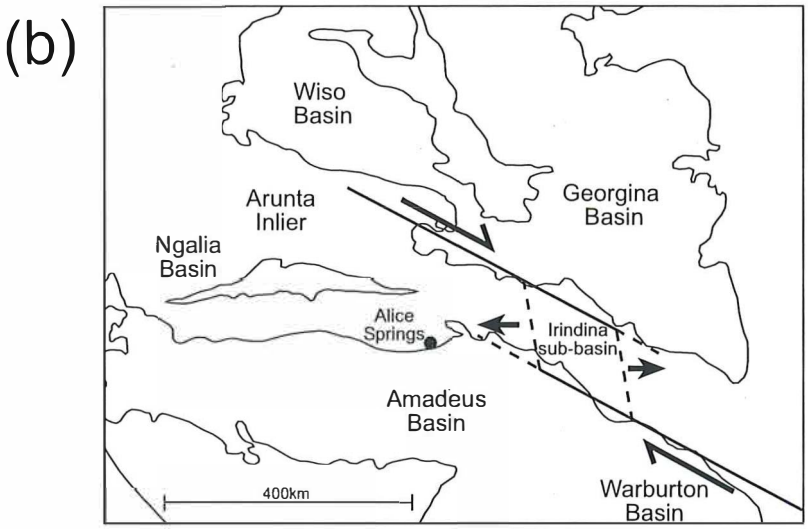

Figure 2: (a) 3D model of the strike-slip Irindina sub-basin at 480Ma showing an intrusion in the Upper Stanovos Gneiss occurring at 520Ma. The strike-slip basin is bounded by deep steeply dipping faults. The diagram shows the Amadeus Basin and the Irindina Supracrustal Assemblage correlatives and the thickness variance betweeen the two sequences.
(b) Basin locality map of central Australia, showing the present day Georgina and Amadeus basins and the protolith to the Irindina Supracrustal Assemblage of the Harts Range, the Irindina sub-basin. The deep strike-slip basin formed as a result of dextral transtensional rifting.

Figure 3

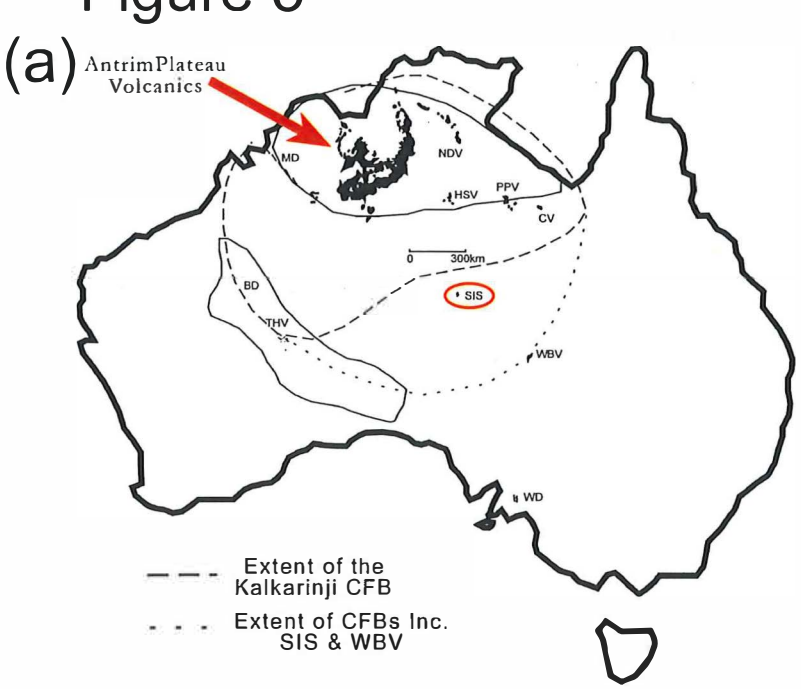

Figure 3a. Extent of early cambrian mafic magmatims throughout Australia. Dashed lines indicate extent of the Kalkarinji continental flood basalts defined by Glass & Phillips, 2001.
MD=Milliwindi Dolerite Dykes, NDV=Nutwood Downs Volcs., HSV =Helen Springs Volcs., PPV=Peake Piker Volcs., CV=Colless Volcs., SIS= Stanovos Igneous Suite, WBV=Warburton Basin Volcs., WD= Woodside Dykes, BD=Boondawari Dolerite, THV=Table Hill Volcs.

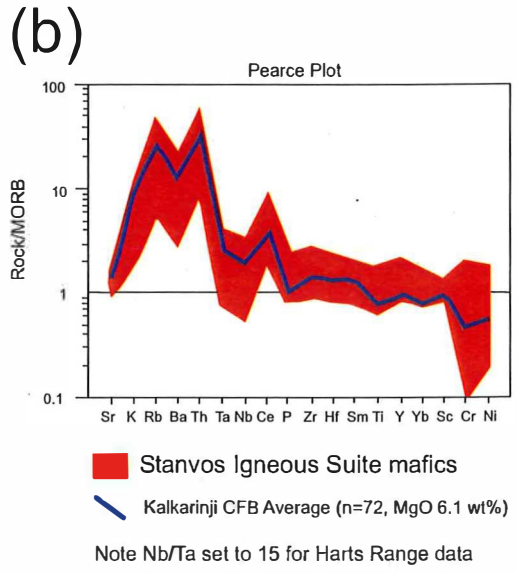

Figure 3b. Multi-element diagram comparison between SIS and the Kalkarinji CFB. There is some scatter caused by element mobilization, however the SIS still show the characteristic Kalkariji CFB geochemical signature.

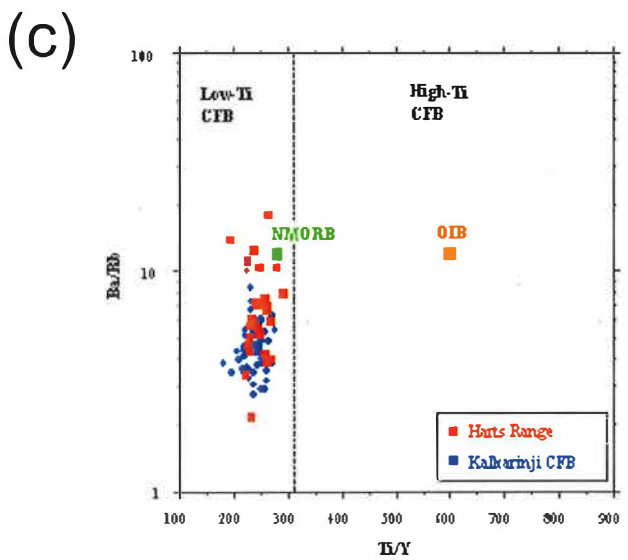

Figure 3c: A Ba/Rb - Ti/Y trace element ratio discrimination diagram

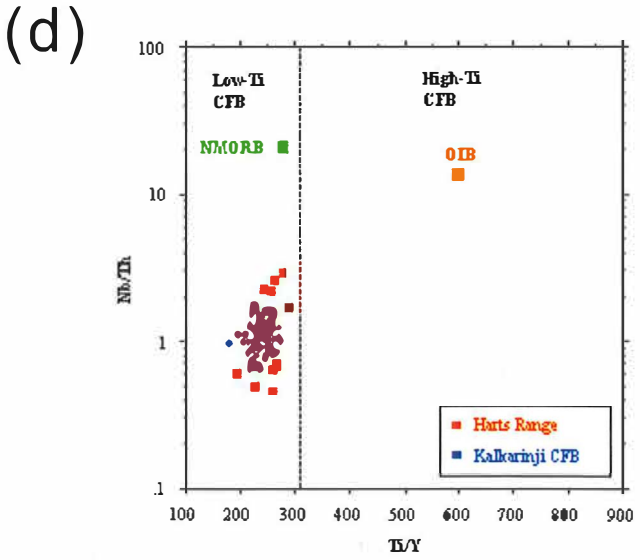

Figure 3: A Nb/Th - Ti/Y trace element ratio discrimination diagram

Figure 4

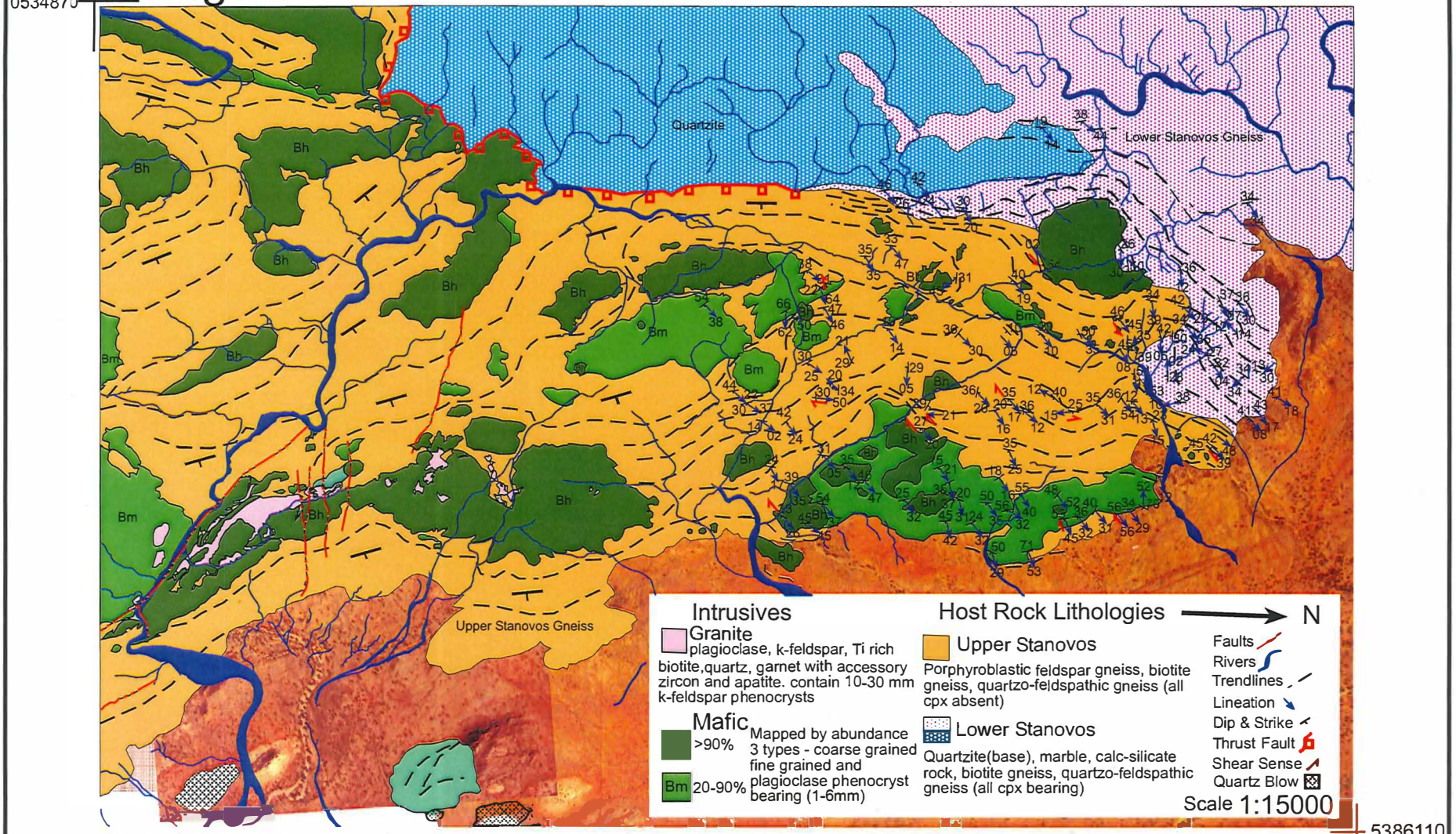

Figure 4: Geological map of the Stanovos Igneous Suite, Harts Range, central Australia

Figure 5

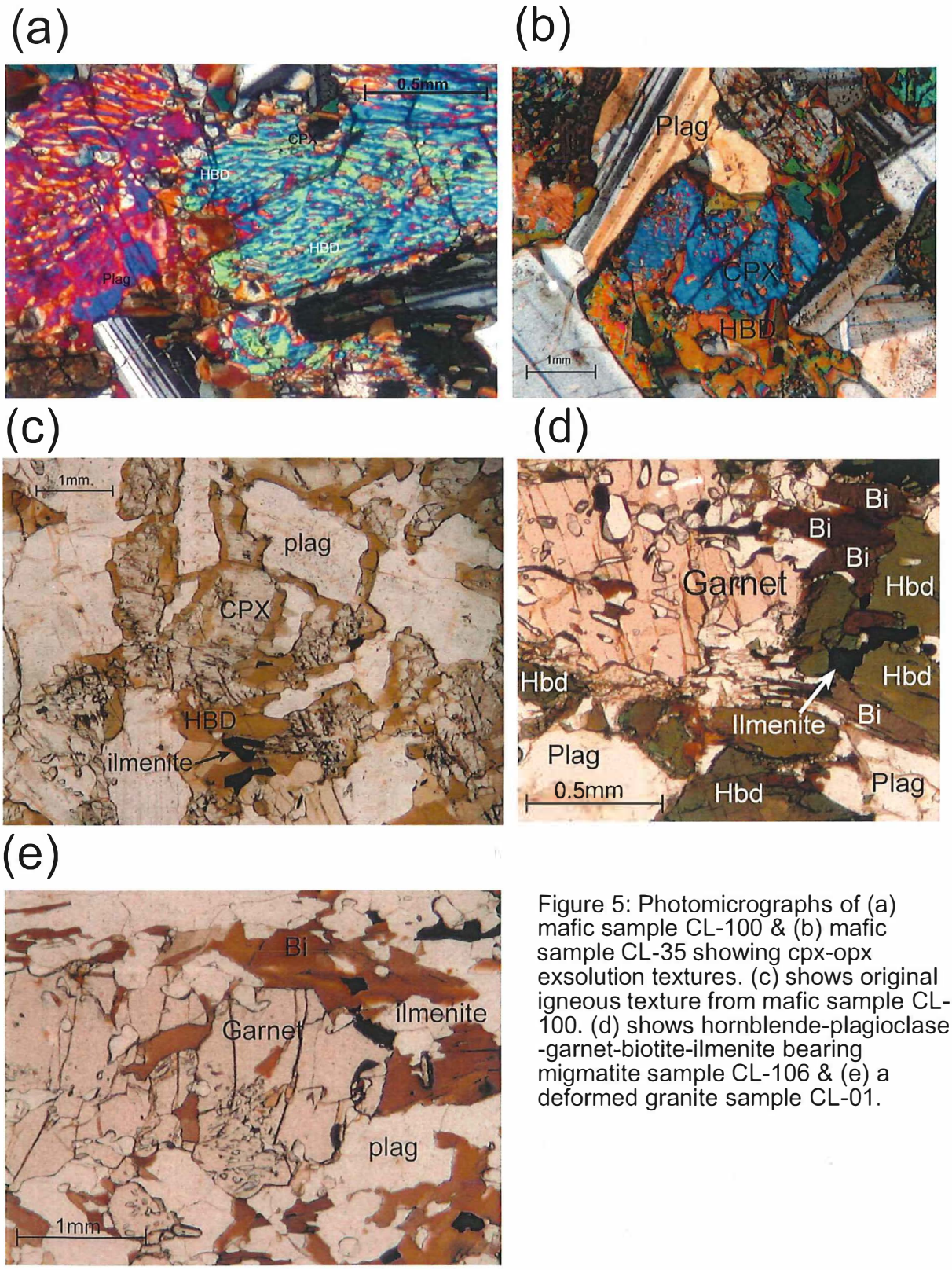

Figure 5: Photomicrographs of (a) mafic sample CL-100 & (b) mafic sample CL-35 showing cpx-opx exsolution textures. (c) shows original igneous texture from mafic sample CL-100. (d) shows hornblende-plagioclase -garnet-biotite-ilmenite bearing migmatite sample CL-106 & (e) a deformed granite sample CL-01.

Figure 6

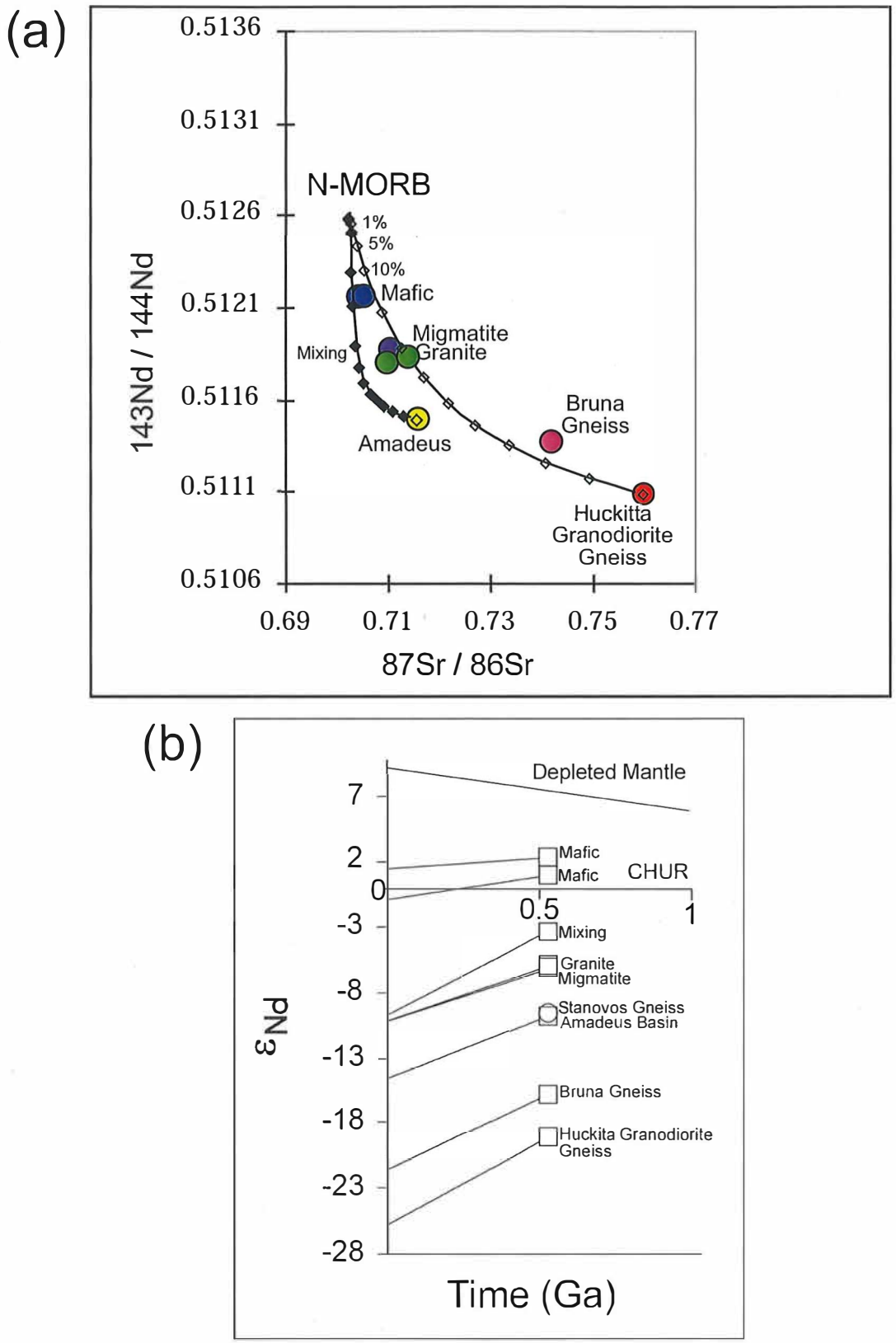

Figure 6: (a) a simple two component (Nd and Sr isotopic compositions) mixing diagram between NMORB and the Huckitta Granodiorite (basement) & NMORB and the Amadeus equivalent (hostrock). (b) Epsilon Nd time evolution diagram for the Stanovos Igneous Suite mafics, mixed rocks adn granite plus the associated migmatite. CHUR = Chrondrite normalised Earth.

Figure 7

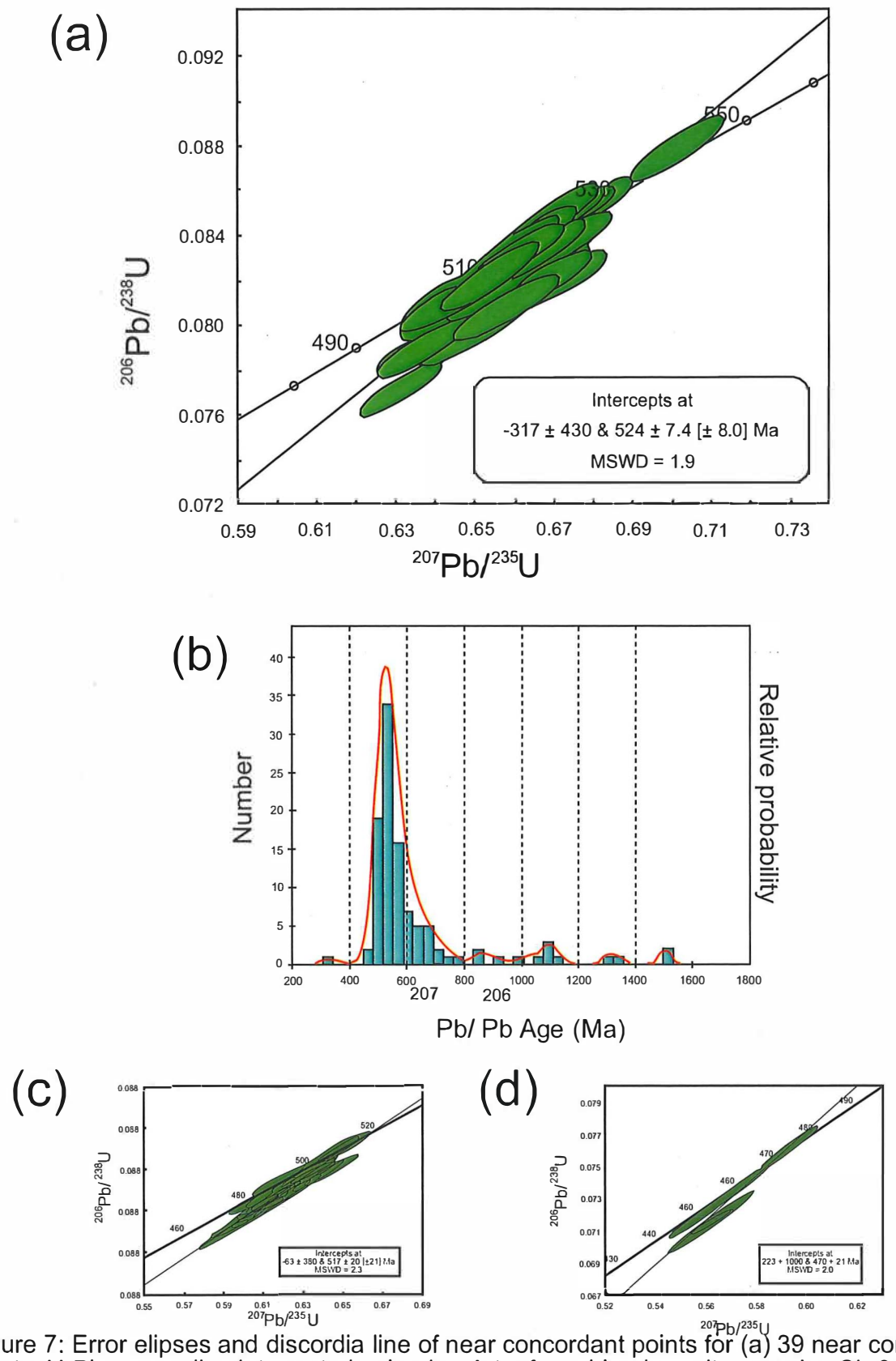

Figure 7: Error elipses and discordia line of near concordant points for (a) 39 near concordant points. U-Pb concordia plot created using Isoplot, of combined granite samples CL-01 and CL-99. The granites have an age of 524+8Ma. (b) probability density plot of 106 zircons from samples CL-01 and CL-99. (c) migmatite 470+24Ma xircons from CL-106 (Larapinta Event) (d) migmatite 517+21Ma zircons from sample CL-106 (Stanovos Event).

Figure 8

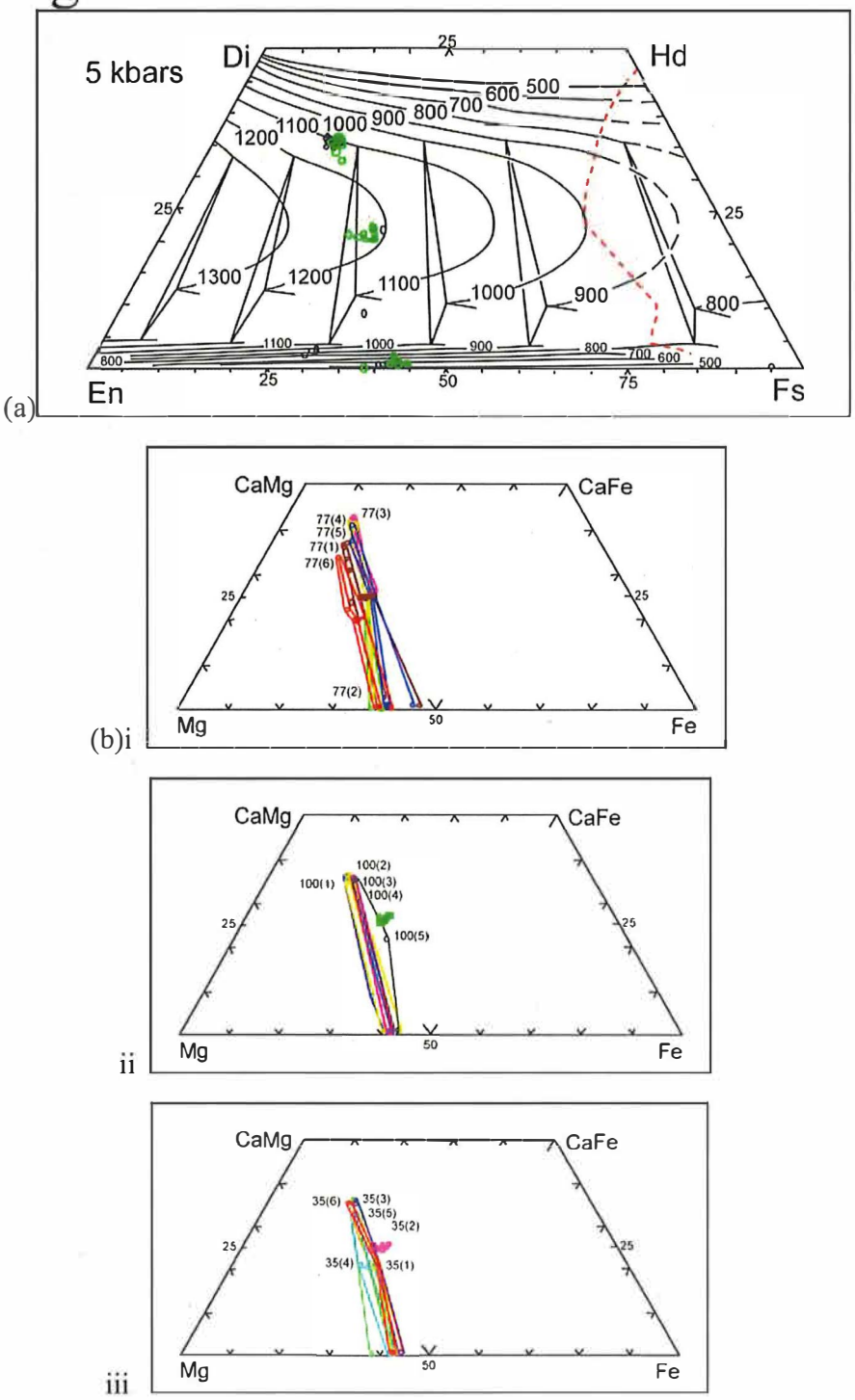

Figure 8: (a) Clinopyroxene-orthopyroxene tielines. Circles denote pyroxene, squares denote hornblende. (b) Wo-En-Fs compositions of coexisting exsolved pyroxenes. The contours indicated polythermal orthopyroxene + augite, orthopyroxene + augite + pigeonite, at 100ºC intervals for use in geothermometry. To the right of the dashed curve indicates metastable zone with respect to augite, olivine and silica. The temperatures were contoured for 5kbar pressures (Lindsley, 1983).

Figure 9

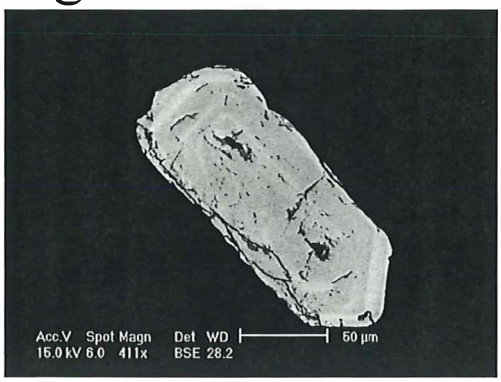

(a)

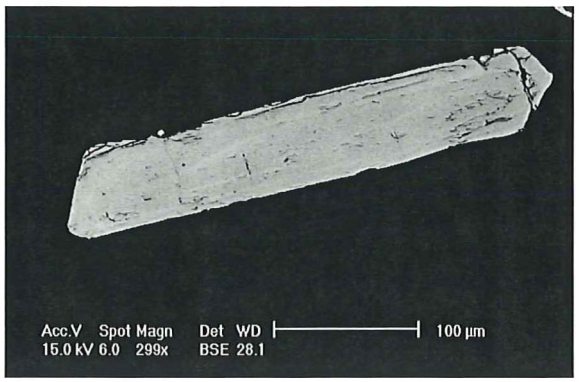

(b)

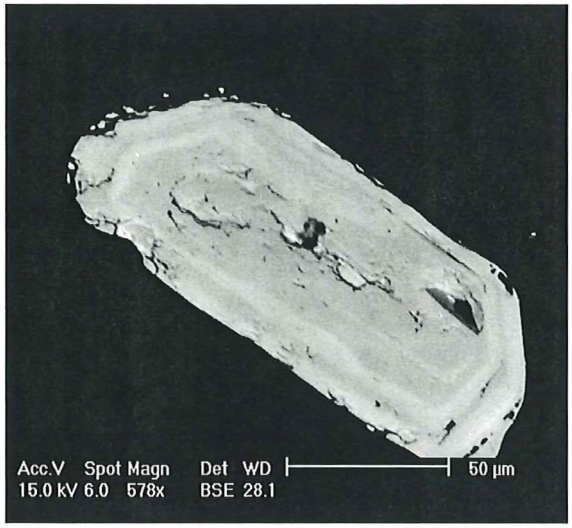

(c)

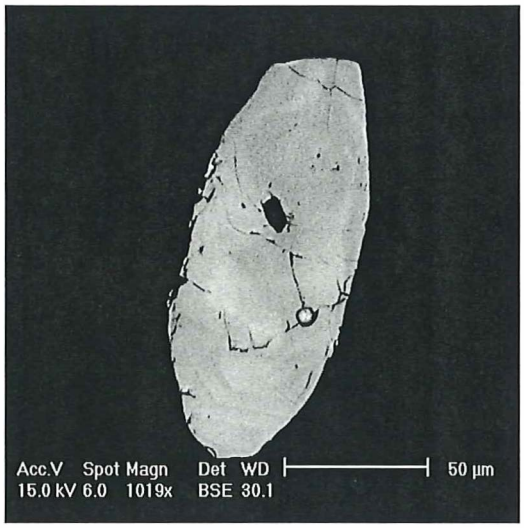

(d)

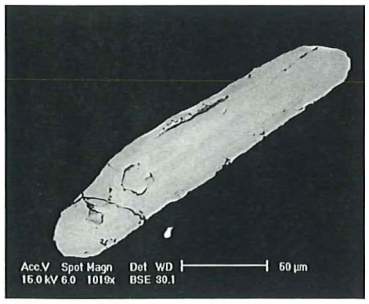

(e)

(f)

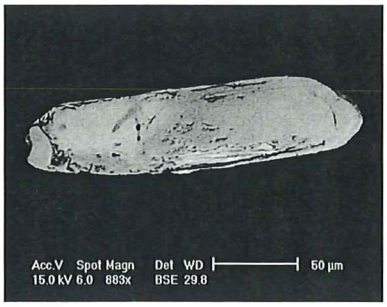

(g)

Figure 9: Backscattered electron images of zircons in sample from crosscutting granite CL-01 (a), (b), (c) migmatite CL-106 (d), (e) crosscutting granite CL-99 (f) & (g). Zircons have a width ranging from 30-60µm and a length ranging from 150 - 400µm. Zoning is clearly seen in (a), (c) & (f) whereas (d) and (g) have zonation that has been smeared.

Figure 10

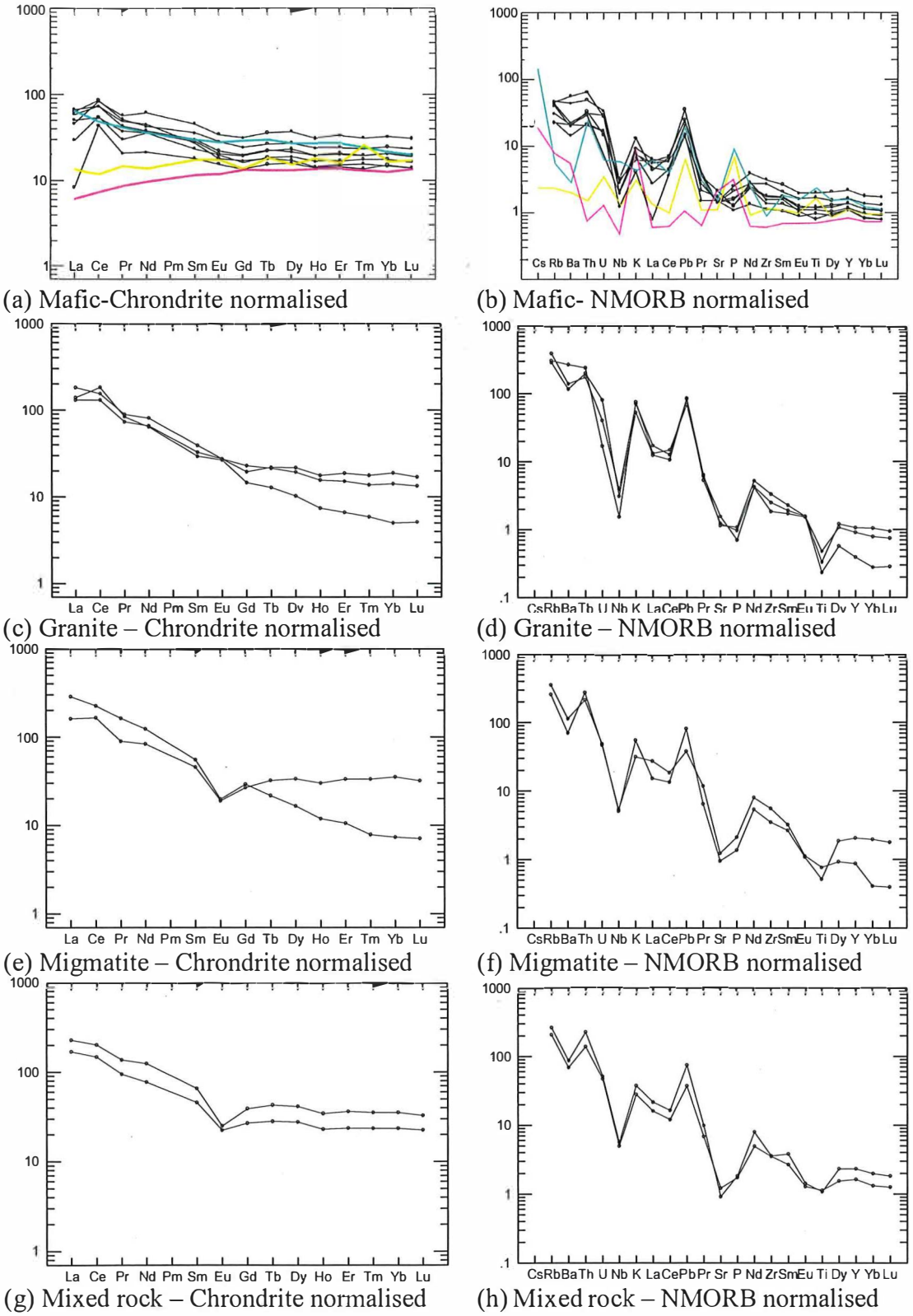

(a) Mafic-Chrondrite normalised

(b) Mafic- NMORB normalised

(c) Granite – Chrondrite normalised

(d) Granite – NMORB normalised

(e) Migmatite – Chrondrite normalised

(f) Migmatite – NMORB normalised

(g) Mixed rock – Chrondrite normalised

(h) Mixed rock – NMORB normalised

Figure 10: Multi-element diagrams normalised to Chrondrite (a,c,e & g) and NMORB (b,d,f & h) for the Stanovos Igneous Suite (Sun & McDonald 1989). Figure (a) and (b) show a comparison with NMORB and the Oman rifted margin Tethyan plume related basalts where blue line = Dolerite Oman group 3, pink line = basalt Oman group 1 and yellow line = NMORB.

Figure 11

(a)

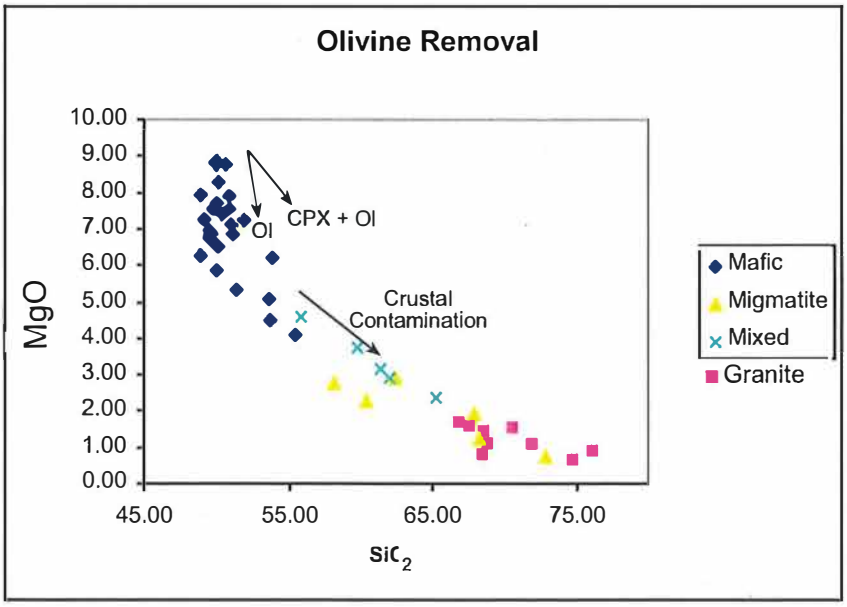

Figure 11a: The negative trend implies olivine removal followed by clinopyroxene removal.

(b)

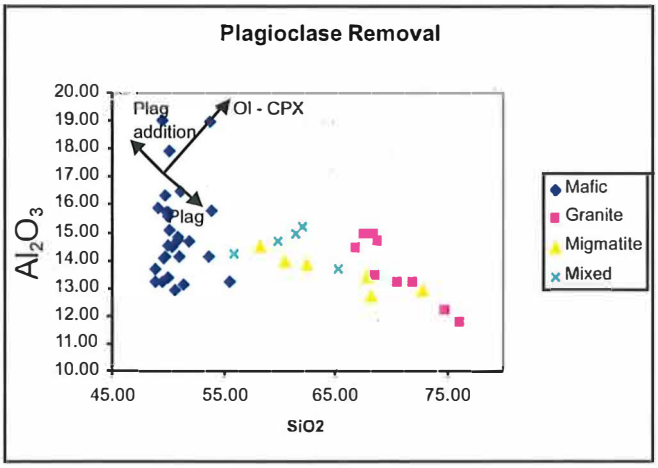

Figure 11b: The initial increase with increasing SiO2 indicating that clinopyroxene + olivine first crystallised without plagioclase. This was followed by Al2O3 depletion indicating the major role of plagioclase fractionation

(c)

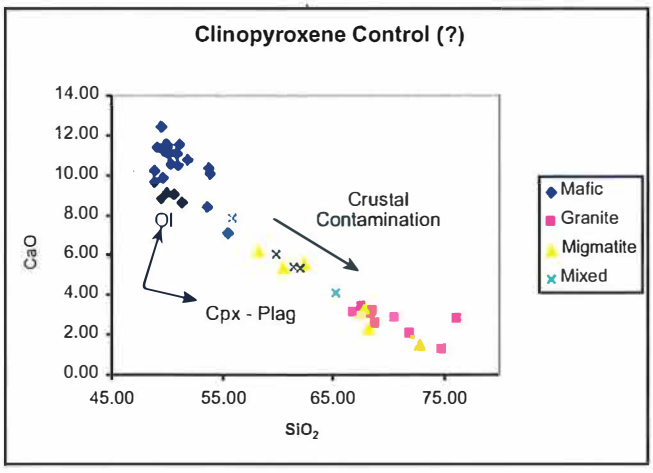

Figure 11c: Show very slight initial increase with increasing SiO2, but is mostly depleted suggesting the important role of clinopyroxene.

Figure 12

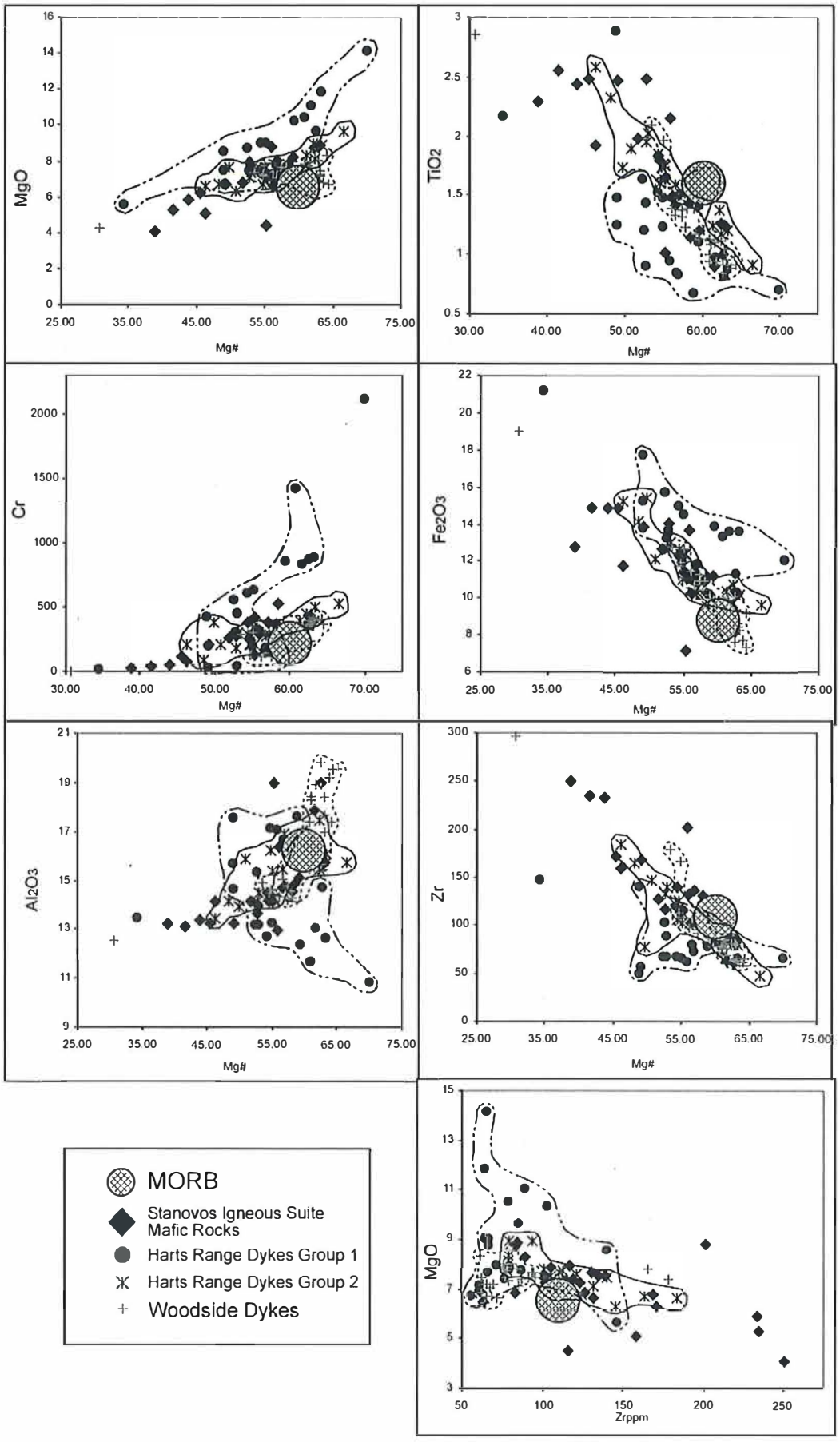
MgO
Mg#
TiO2
Mg#
Cr
Mg#
Fe2O3
Mg#
Al2O3
Mg#
Zr
Mg#
MgO
Zrppm
MORB
Stanovos Igneous Suite Mafic Rocks
Harts Range Dykes Group 1
Harts Range Dykes Group 2
Woodside Dykes

Figure 13

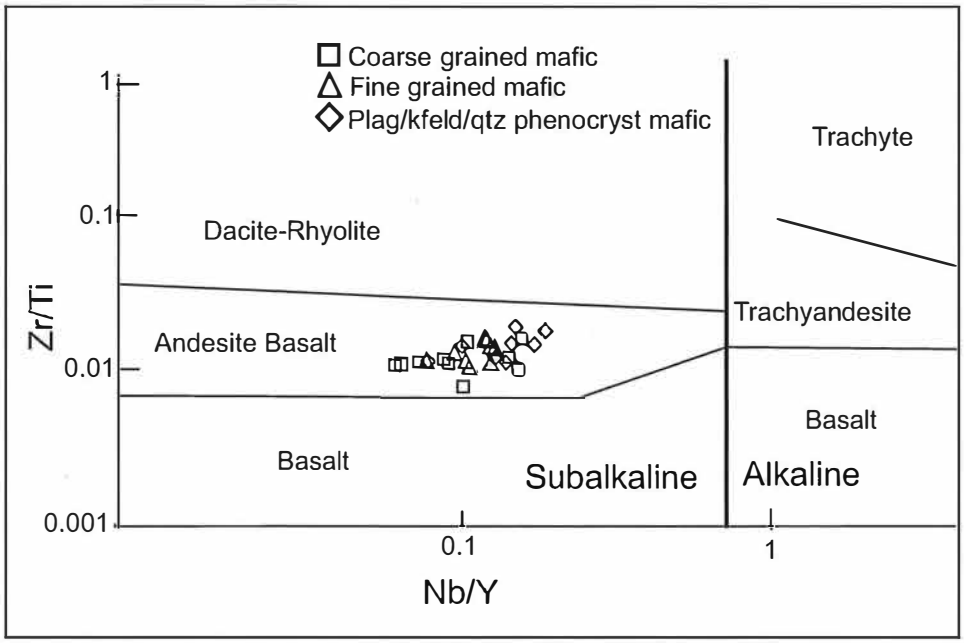

Figure 13a: Zr/Ti-Nb/Y, boundaries from Winchester & Floyd (1977). Incompatible trace element ratios from the Stanovos Igneous Suite plot as subalkaline in the andesite basalt field. The mafic rocks progressively become more alkalic from coarse grained mafics to fine grained mafics through to plagioclase phyric mafics.

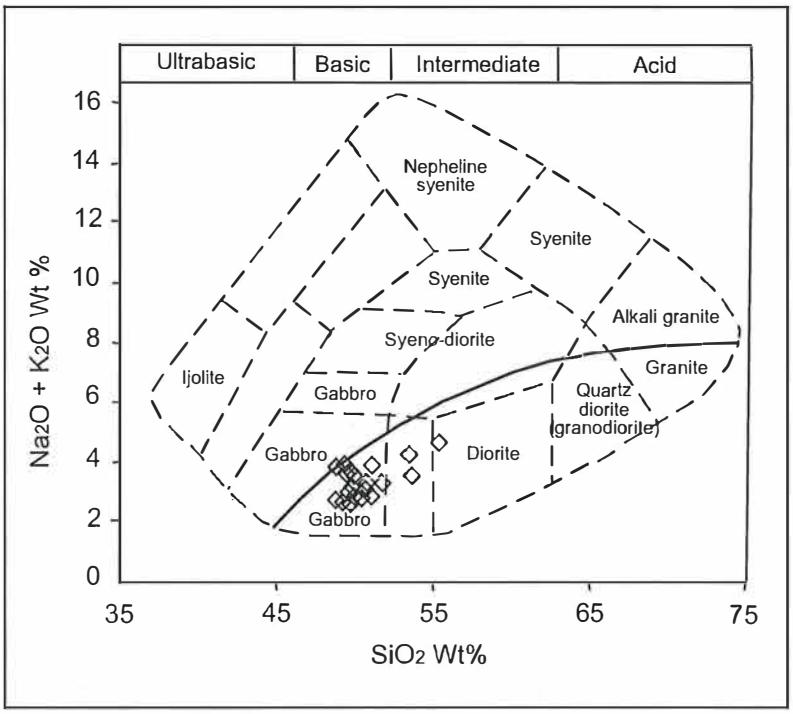

Figure 13b: Chemical classification and nomenclature of plutonic rocks using totall alkalis vs silica (TAS) diagram of Cox et al. (1979). The curved solid line subdivides alkalic from subalkalic rocks. Mafic rocks from the Stanovos Igneous Suite plot in the subalkalic (tholeiitic) gabbro field.

Figure 14

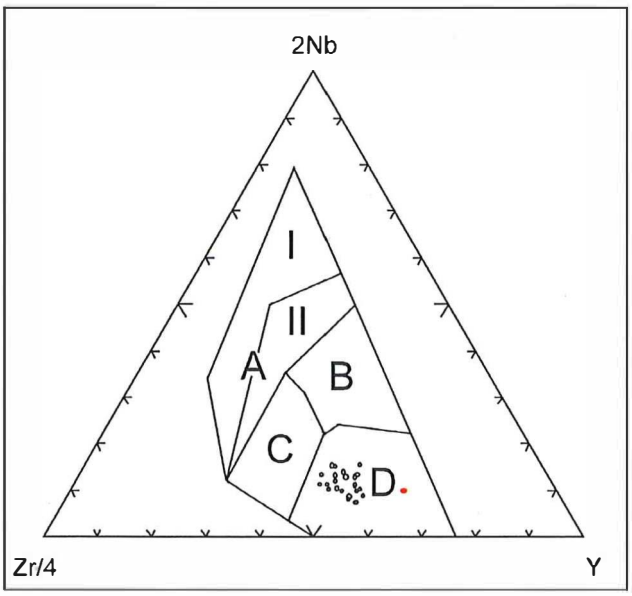

Figure 14a: Mafic rock samples plotted on the Zr-Nb-Y discrimination diagram for basalts (Hugh Rollinson, 1993). All mafic rock samples plotted in the D field indicating N-type MORB and volcanic-arc basalts. The solid red dot indicates a mafic dyke sampled approx. 15.3km NNE of the field area. The remaining fields represent the following: AI, within-plate alkali basalts; AII, within-plate alkali basalts and within plate tholeiites; B, E-type MORB; C, within-plate tholeiites and volcanic-arc basalts.

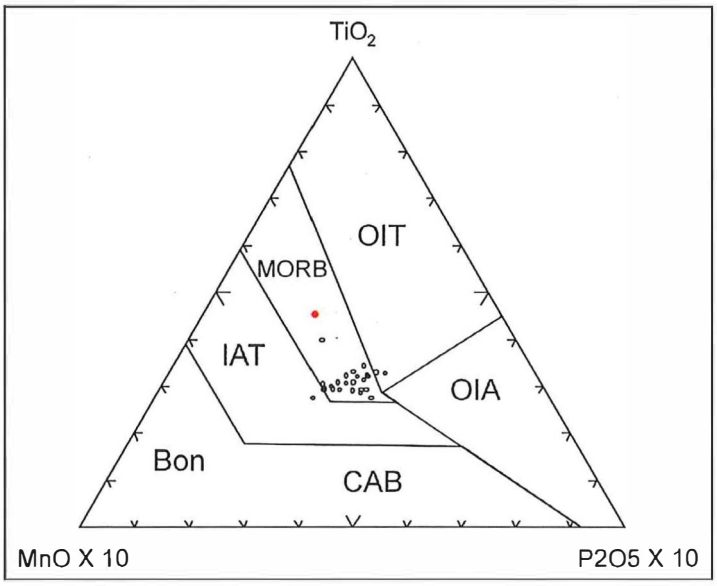

Figure 14b: Mafic rock samples plotted on the MnO-TiO2-P2O5 discrimination diagram for basalts and basaltic andesites (Hugh Rollinson, 1993). Mafic rock samples predominantly lye within the MORB field. The solid red dot indicates a mafic dyke sampled approx 15.3km NNE of the field area. The remaining fields are as follow: OIT, ocean-island tholeiite or seamount tholeiite; OIA, ocean-island alkali basalt or seamount alkali basalt; CAB – island-arc calc-alkaline basalt; IAT- island-arc tholeiite; Bon, boninite.

Figure 15

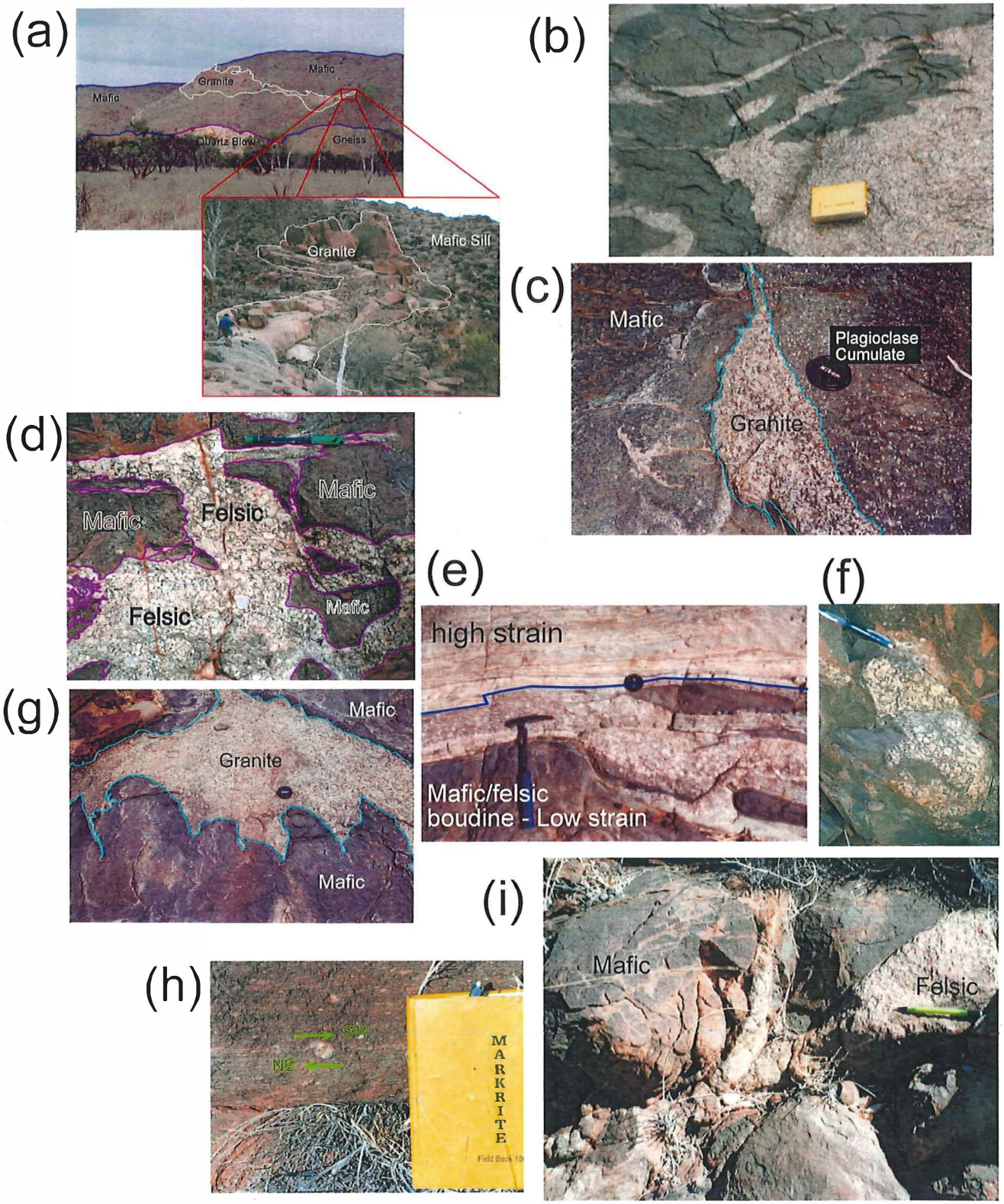

Figure 15: (a) large scale mafic granite intrusions and their crosscutting relationships. (b) Fragmented mafic indicated mafic crystallised before granite. (c) Plagioclase phyric rock cumulative textures. (d) GPS (Datum = WGS 84, Coords = UTM UPS) locality (0536651/7426033), facing south, same relationship as (b). (e) (0536736/7425161) facing west. Same relationship as (b) and (d) only in the form of a boudin surrounded by highly strained Upper Stanovos Gneiss host rock.(f) (0536872/7424909) facing north. mingling between mafic and granite, granite portion is extremely coarse grained, clasts up to 3cm. (g) Melt mixing textures showing scalloped boundaries. The boundary between the felsic and mafic rocks are quenched. (h) (0536679/7425609) looking southeast. Dextral delta clast showing a top towards southwest shearsense. (i) (0536155/7425116) looking northwest. Granite cross cutting mafic occuring on a smale scale.

Figure 16

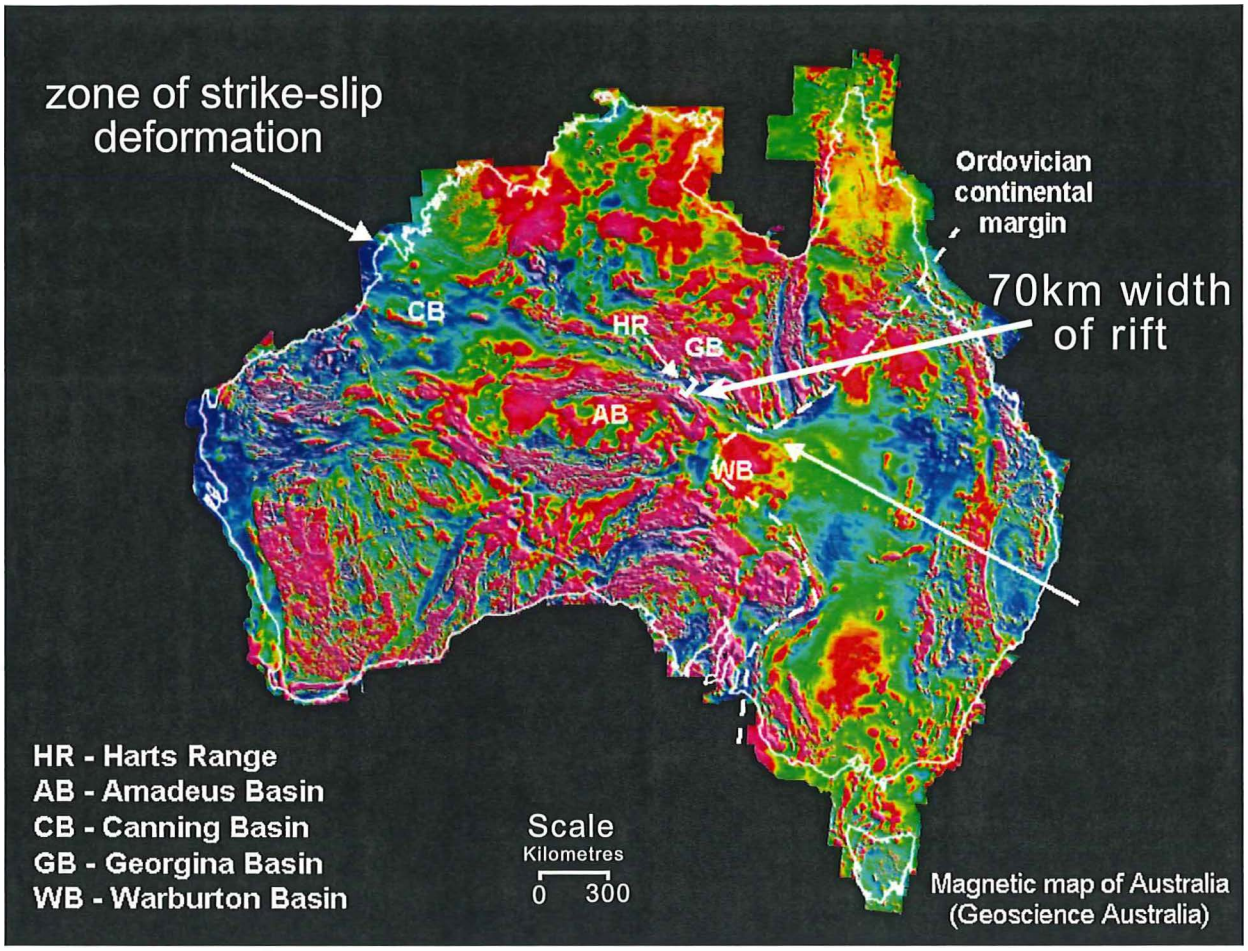

Figure 16: Magnetic map of Australia featuring northwest (Canning Basin) to southeast (Warburton Basin) prominent linear feature containing rift related Cambrian volcanics.The width of the rift is depicted as 70km wide.

Table 1 Major and trace element data for the crosscutting granites

	GRANITES									MIGMATITE					
Sample	CL-01	CL-02	CL-37	CL-39	CL-56	CL-73(B)	CL-82	CL-99	CL-108	CL-59	CL-85	CL-87	CL-91	CL-102	CL-106
SiO2	68.40	68.62	71.99	74.77	67.62	70.51	76.15	68.82	66.88	58.18	67.88	72.75	68.23	62.40	60.34
Al2O3	14.91	13.42	13.20	12.21	14.91	13.16	11.73	14.68	14.40	14.49	13.40	12.87	12.68	13.81	13.94
Fe2O3T	2.71	6.21	3.54	1.69	5.05	4.90	2.28	3.69	5.57	11.70	5.53	3.14	3.49	7.90	10.26
MnO	0.04	0.10	0.05	0.03	0.06	0.08	0.03	0.05	0.10	0.17	0.07	0.04	0.05	0.13	0.15
MgO	0.81	1.44	1.06	0.63	1.59	1.55	0.90	1.07	1.68	2.74	1.91	0.74	1.24	2.93	2.28
CaO	3.04	3.19	1.99	1.28	3.42	2.84	2.78	2.56	3.09	6.16	3.23	1.49	2.30	5.57	5.32
Na2O	2.97	1.74	2.51	2.17	3.36	2.57	2.94	2.71	2.29	2.54	2.70	2.73	2.60	3.31	3.14
K2O	3.83	3.93	4.65	5.47	2.59	2.90	1.15	5.15	3.86	1.71	2.27	4.71	3.98	1.29	1.89
TiO2	0.42	1.10	0.59	0.30	0.85	0.85	0.41	0.61	0.88	2.27	0.97	0.51	0.65	1.85	1.85
P2O5	0.11	0.18	0.11	0.08	0.21	0.18	0.06	0.13	0.18	0.29	0.25	0.12	0.16	0.15	0.44
SO3	0.01	0.01	0.01	0.01	0.01	0.01	0.00	0.01	0.01	0.01	0.01	0.01	0.01	0.01	0.02
LOI	0.17	-0.02	0.18	0.25	0.28	0.14	0.34	0.27	0.50	-0.12	0.38	0.36	0.26	0.60	0.17
Total	97.42	99.91	99.88	98.88	99.97	99.67	98.78	99.73	99.46	100.14	98.59	99.45	95.63	99.93	99.80
Mg#	37.19	31.40	37.32	42.65	38.42	38.46	43.91	36.38	37.41	31.71	40.57	31.71	41.23	42.33	30.54
Zr	183.9	206.2	286.3	136.4	362.0	310.7	224.9	245.4	240.6	158.6	410.2	229.7	257.6	91.0	351.2
Nb	7.2	11.0	10.0	3.6	11.4	12.8	2.6	9.1	13.3	14.6	12.5	8.8	11.8	19.1	16.4
Y	40.8	35.3	33.2	13.0	38.8	45.7	7.5	30.9	44.2	65.6	24.3	49.2	57.3	150.4	73.4
Sr	110.6	76.3	70.1	140.5	117.6	81.8	140.5	103.0	95.9	117.2	110.9	84.8	85.5	154.4	140.5
Rb	160.6	134.4	178.3	171.7	121.6	141.5	69.8	217.8	156.3	88.6	143.9	189.2	197.8	62.2	110.8
U	3.8	2.5	2.2	0.8	2.6	4.0	0.9	1.9	4.2	4.2	2.2	2.2	2.3	4.5	2.2
Th	24.0	8.4	42.0	28.9	30.8	22.4	3.0	21.0	12.7	26.2	32.9	35.7	25.6	4.7	29.1
Pb	25.1	22.4	31.6	20.6	21.3	22.3	12.2	25.6	26.8	18.2	11.4	19.5	24.3	9.4	16.9
Ga	19.9	20.5	16.8	13.0	20.5	17.9	14.0	19.8	19.8	22.9	19.4	16.0	17.3	18.2	23.0
Cu	8	9	2	3	14	8	25	7	12	18	17	3	4	18	11
Zn	31	68	48	20	54	52	24	38	69	115	67	44	41	74	108
Ni	8	8	9	5	12	15	7	8	13	16	14	6	10	18	9
Ba	735	485	653	1687	611	605	379	880	870	275	445	669	716	235	507
Sc	8.4	13.6	10.6	3.2	12.4	11.7	3.7	7.6	13.3	31.7	7.2	9.1	9.1	29.9	24.8
Co	45	63	53	68	42	58	61	49	61	69	48	39	45	53	40
V	52	126	73	38	94	110	43	68	113	310	111	48	79	306	190
Ce	80	56	151	112	131	68	21	95	75	94	138	119	101	42	115
Nd	31	31	69	30	54	27	6	38	36	49	58	54	39	31	54
La	31	27	80	33	61	22	5	43	30	42	68	65	38	6	49
Cr	18	12	24	13	35	37	13	26	37	12	35	14	25	28	14
Zr/Nb	25.54	18.75	28.63	37.89	31.75	24.27	86.50	26.97	18.09	10.86	32.82	26.10	21.83	4.76	21.41
Th/Nb	3.33	0.76	4.20	8.03	2.70	1.75	1.15	2.31	0.95	1.79	2.63	4.06	2.17	0.25	1.77
Zr/Y	4.51	5.84	8.62	10.49	9.33	6.80	29.99	7.94	5.44	2.42	16.88	4.67	4.50	0.61	4.78

All oxide values are expressed as wt%. Trace elements expressed as ppm. Co is subject to mill contamination. All zero values represent values which fall below detection limits. Mg# = [(Mg/ (Mg+ Fe))*100]. LOI: denotes loss on ignition.

Table 2 Major and trace element Data for the Mafic rocks

	MAFIC PLAG								MAFIC COARSE								
Sample	CL-15	CL-31	CL-33	CL-42	CL-66	CL-70	CL-72	CL-101	CL-35	CL-49	CL-65	CL-75	CL-76	CL-77	CL-79	CL-100	CL-116	CL-119
SiO2	50.81	49.67	49.06	55.43	51.13	50.09	53.73	49.50	50.54	50.78	51.87	49.93	49.91	49.81	49.42	50.03	53.78	48.87
Al2O3	14.75	16.32	15.87	13.23	16.46	17.90	18.98	13.23	12.93	14.84	14.67	15.59	15.71	15.71	19.00	15.07	15.76	13.66
Fe2O3T	11.26	10.28	10.31	12.74	9.20	8.00	7.15	13.85	13.72	11.13	10.98	10.41	10.29	10.31	8.21	11.24	8.70	14.01
MnO	0.19	0.17	0.17	0.19	0.16	0.14	0.12	0.22	0.22	0.19	0.19	0.17	0.17	0.17	0.14	0.19	0.15	0.22
MgO	7.52	6.65	7.25	4.09	6.87	6.48	4.46	6.76	8.77	7.86	7.22	8.76	8.88	8.83	6.94	8.26	6.20	7.92
CaO	11.06	11.27	11.38	7.07	11.54	11.17	10.35	8.79	9.00	11.04	10.76	11.34	11.48	11.48	12.38	11.04	10.04	10.17
Na2O	2.54	3.02	3.11	2.70	2.31	2.80	2.82	2.57	2.36	2.55	2.80	2.39	2.31	2.33	2.34	2.50	2.59	2.42
K2O	0.54	0.60	0.73	1.92	0.54	0.76	0.68	1.37	0.45	0.36	0.52	0.36	0.30	0.30	0.31	0.36	0.97	0.27
TiO2	1.51	1.49	1.43	2.30	1.21	0.90	1.02	2.47	2.15	1.55	1.42	1.26	1.23	1.24	1.00	1.41	1.14	2.48
P2O5	0.19	0.19	0.19	0.28	0.14	0.10	0.15	0.25	0.25	0.16	0.15	0.13	0.13	0.13	0.10	0.14	0.12	0.15
SO3	0.04	0.01	0.02	0.03	0.03	0.06	0.01	0.03	0.02	0.02	0.02	0.02	0.01	0.01	0.01	0.03	0.02	0.04
LOI	-0.10	0.28	0.24	0.00	0.42	1.59	0.40	0.50	-0.24	-0.10	-0.13	-0.09	0.00	-0.02	0.02	-0.09	0.32	-0.13
Total	100.31	99.96	99.77	99.97	99.99	99.97	99.86	99.55	100.17	100.38	100.45	100.27	100.42	100.30	99.89	100.17	99.77	100.08
Mg#	56.95	56.16	58.22	38.89	59.67	61.60	55.28	49.16	55.87	58.30	56.55	62.50	63.07	62.91	62.60	59.28	58.52	52.81
Zr	135.4	132.2	123.5	250.5	83.6	63.9	116.7	168.4	201.6	105.3	102.4	83.2	84.6	83.8	61.4	90.0	105.8	116.8
Nb	6.6	5.5	3.7	11.1	2.3	3.0	4.6	7.0	7.2	2.7	4.7	2.0	2.8	2.9	3.5	2.1	3.2	3.7
Y	39.6	38.2	35.8	61.4	27.9	23.3	31.3	50.6	46.2	34.8	33.1	29.2	30.3	30.7	23.2	31.7	30.0	35.4
Sr	129.3	141.7	136.5	119.5	159.3	165.7	195.2	152.2	130.5	134.5	158.1	132.5	135.7	137.1	159.3	146.8	150.0	148.2
Rb	22.4	19.8	8.3	88.4	18.5	42.1	25.8	83.4	12.7	13.5	17.4	14.6	12.0	12.9	12.5	14.2	37.1	6.2
U	0.7	2.4	0.8	2.0	0.8	1.1	1.3	2.1	0.8	1.0	-0.5	1.0	-0.1	0.8	1.3	0.4	1.0	-0.1
Th	4.0	4.3	2.5	11.4	3.6	4.5	7.8	4.2	2.5	4.0	3.5	4.4	2.4	2.6	1.6	3.1	6.4	3.0
Pb	4.2	5.4	4.7	13.2	2.1	5.2	10.7	8.3	7.5	3.2	6.4	3.1	1.3	4.5	1.7	5.1	7.1	5.2
Ga	19.6	15.2	14.8	21.7	18.2	15.0	18.2	20.1	19.1	18.0	18.7	18.6	16.2	15.5	17.2	19.3	18.6	19.8
Cu	54	50	40	23	36	46	14	45	78	59	41	50	55	55	57	66	35	78
Zn	85	83	83	120	67	60	59	122	117	87	83	77	75	75	56	81	70	111
Ni	75	63	73	18	46	44	26	66	165	93	35	102	113	116	96	79	35	112
Ba	126	121	104	412	124	92	359	670	132	81	132	57	67	92	53	57	159	146
Sc	41.7	38.6	39.2	36.7	41.0	36.4	28.7	47.0	43.6	42.5	40.1	38.2	39.4	39.0	32.7	40.1	36.3	48.9
Co	54	49	52	50	47	39	46	53	67	57	61	71	60	61	48	57	51	61
V	291	264	258	338	245	213	177	395	338	290	280	258	258	258	201	279	240	457
Ce	45	42	33	88	31	21	45	52	53	36	34	27	22	27	23	28	36	35
Nd	18	19	13	39	13	8	21	22	20	14	17	11	10	10	9	14	13	10
La	14	9	7	36	3	5	16	14	15	6	7	5	4	2	3	5	10	6
Cr	383	302	359	20	322	309	135	208	294	525	177	368	392	392	416	333	260	277
Zr/Nb	20.52	24.04	33.38	22.57	36.35	21.30	25.37	24.06	28.00	39.00	21.79	41.60	30.21	28.90	17.54	42.86	33.06	31.57
Th/Nb	0.61	0.78	0.68	1.03	1.57	1.50	1.70	0.60	0.35	1.48	0.74	2.20	0.86	0.90	0.46	1.48	2.00	0.81
Zr/Y	3.42	3.46	3.45	4.08	3.00	2.74	3.73	3.33	4.36	3.03	3.09	2.85	2.79	2.73	2.65	2.84	3.53	3.30

All oxide values are expressed as wt%. Trace elements expressed as ppm. Co is subject to mill contamination. All zero values represent values which fall below detection limits. Mg# = [(Mg/ (Mg+ Fe))*100]. LOI: denotes loss on ignition.

Table 3 Major and trace element data for mafics, mixed and miscellaneous

	MAFIC FINE								MIXING						MAFIC DYKE	PEGMATITE	Gt Calc Sil
Sample	CL-40	CL-41	CL-48	CL-74	CL-83	CL-86	CL-98	CL-104	CL-110	CL-08	CL-09	CL-55	CL-84	CL-93	CL-80	CL-109	CL-78
SiO2	51.29	50.01	50.36	49.57	50.93	49.94	53.61	49.68	48.87	61.99	61.44	55.76	59.82	65.27	47.61	72.77	43.11
Al2O3	13.11	13.38	14.48	14.10	14.11	14.55	14.13	14.12	13.24	15.16	14.92	14.25	14.66	13.69	12.92	15.02	23.88
Fe2O3T	14.86	14.83	12.34	12.65	11.43	10.90	11.72	12.43	14.90	7.37	8.07	10.85	8.29	7.62	10.73	1.62	10.24
MnO	0.23	0.24	0.20	0.21	0.19	0.18	0.19	0.20	0.24	0.11	0.13	0.17	0.13	0.13	0.19	0.03	0.09
MgO	5.32	5.87	7.39	6.86	7.10	7.67	5.09	7.54	6.27	2.93	3.16	4.57	3.75	2.38	13.53	0.71	1.06
CaO	8.57	9.05	10.50	9.86	10.44	11.19	8.40	11.15	9.64	5.34	5.40	7.82	6.06	4.09	11.64	3.81	18.63
Na2O	2.87	2.87	2.58	3.23	2.55	2.62	2.89	2.58	2.74	2.53	2.41	2.78	2.64	2.35	1.50	3.99	1.33
K2O	0.96	0.79	0.45	0.72	0.71	0.56	1.34	0.39	1.05	2.79	2.65	1.51	2.01	2.69	0.23	1.03	0.09
TiO2	2.56	2.44	1.84	1.98	1.65	1.55	1.92	1.80	2.48	1.24	1.25	1.75	1.44	1.38	0.60	0.28	0.94
P2O5	0.30	0.28	0.19	0.22	0.18	0.20	0.20	0.20	0.28	0.19	0.20	0.23	0.20	0.21	0.11	0.06	0.24
SO3	0.02	0.03	0.02	0.02	0.01	0.01	0.02	0.02	0.02	0.01	0.01	0.02	0.02	0.01	0.09	0.01	0.01
LOI	0.21	0.32	-0.06	0.25	0.27	0.27	0.21	-0.08	0.23	0.22	0.10	0.37	0.38	0.11	0.57	0.36	0.15
Total	100.30	100.09	100.28	99.66	99.58	99.63	99.70	100.04	99.96	99.87	99.73	100.06	99.40	99.93	99.71	99.68	99.77
Mg#	41.50	43.92	54.27	51.77	55.14	58.20	46.22	54.58	45.46	44.01	43.70	45.45	47.27	38.20	71.41	46.45	16.98
Zr	234.7	233.6	119.7	127.0	115.4	130.7	158.1	139.4	171.2	215.6	231.6	177.5	260.1	264.4	39.1	86.0	403.3
Nb	7.6	7.8	5.3	4.9	3.5	4.9	6.7	4.3	6.4	12.6	12.5	6.6	11.5	13.1	1.7	4.5	19.8
Y	62.1	65.3	42.4	45.0	43.4	39.2	52.0	44.0	60.3	45.7	46.9	52.0	45.4	64.8	21.5	11.9	92.8
Sr	129.0	130.7	137.5	146.9	125.1	134.4	124.8	134.4	138.2	114.4	117.0	119.8	109.3	82.0	56.5	147.7	3046.2
Rb	26.6	21.5	16.3	10.7	26.6	24.3	62.8	14.2	24.8	116.0	106.0	70.2	115.7	146.7	6.2	55.3	5.4
U	1.6	0.0	2.0	0.9	1.1	1.4	0.9	0.1	0.9	3.1	2.2	1.8	2.2	2.4	0.9	1.8	9.1
Th	6.0	4.5	3.4	1.9	5.2	3.8	9.4	1.9	4.0	7.4	7.3	11.4	16.6	27.1	0.3	13.6	45.4
Pb	7.6	12.4	5.0	5.6	6.6	4.3	6.5	5.0	8.5	17.7	20.8	12.1	11.1	22.4	3.3	22.0	4.7
Ga	23.9	23.0	18.7	19.2	17.9	17.1	19.9	18.5	19.1	22.1	21.7	20.0	18.1	21.0	12.1	18.0	81.9
Cu	21	38	50	40	46	58	21	57	57	23	23	36	38	23	24	4	2
Zn	133	135	99	110	97	86	102	98	131	87	93	94	78	84	90	18	6
Ni	23	27	80	70	66	68	26	67	41	22	25	34	28	19	440	7	7
Ba	277	242	113	195	133	141	216	99	129	788	877	279	433	543	79	123	265
Sc	48.7	52.2	44.8	44.3	45.8	43.0	40.7	46.6	51.1	19.1	20.3	37.0	23.9	20.8	44.6	2.7	15.6
Co	50	56	58	54	53	54	56	62	56	56	43	63	58	56	70	58	32
V	415	404	331	337	300	283	322	339	418	194	213	299	208	197	217	34	196
Ce	51	50	39	44	44	33	51	43	48	76	88	62	90	123	16	44	184
Nd	29	28	19	16	19	17	23	19	23	32	45	29	36	58	4	15	92
La	11	18	9	10	11	12	19	8	12	26	42	24	40	54	0	20	119
Cr	39	49	385	259	416	373	75	262	117	68	82	13	88	44	1910	24	17
Zr/Nb	30.88	29.95	22.58	25.92	32.97	26.67	23.60	32.42	26.75	17.11	18.53	26.89	22.62	20.18	23.00	19.11	20.37
Th/Nb	0.79	0.58	0.64	0.39	1.49	0.78	1.40	0.44	0.63	0.59	0.58	1.73	1.44	2.07	0.02	3.02	2.29
Zr/Y	3.78	3.58	2.82	2.82	2.66	3.33	3.04	3.17	2.84	4.72	4.94	3.41	5.73	4.08	1.82	7.23	4.35

All oxide values are expressed as wt%. Trace elements expressed as ppm. Co is subject to mill contamination. All zero values represent values which fall below detection limits. Mg# = [(Mg/ (Mg+ Fe))*100]. LOI: denotes loss on ignition.

Table 4 Rare-earth element data for representative samples for the Stanovos Igneous Suite

rock type	G	Mix	Mp	Mc	G	Mf	Mc	Mp	Mc	Mix	Mig	Mf	Mig	Mix	G	DETECTION
samples	CL-01	CL-08	CL-15	CL-35	CL-39	CL-40	CL-65	CL-72	CL-77	CL-84	CL-85	CL-86	CL-91	CL-93	CL-99	LIMIT
Ce	76	74	36.5	43	120	44	24	43.5	16.5	96	170	31.5	105	130	100	0.5
Dy	5.5	8	5.5	7	2.6	9.5	4.8	4.4	4.1	7	4.2	6	8.5	10.5	4.9	0.02
Er	3.1	4.4	3.4	4	1.1	5.5	2.8	2.5	2.4	3.9	1.75	3.3	5.5	6	2.5	0.05
Eu	1.6	1.9	1.3	1.65	1.55	2	1.15	1.05	0.91	1.3	1.15	1.2	1.1	1.45	1.6	0.02
Gd	4	6	4.1	5	3	6.5	3.4	3.5	2.8	5.5	6	4	5.5	8	4.7	0.05
Ho	1	1.5	1.1	1.35	0.42	1.75	0.94	0.82	0.8	1.3	0.67	1.1	1.7	1.95	0.88	0.02
La	28.5	25	13.5	15.5	33.5	13	8.5	15.5	5.5	39.5	74	11.5	34.5	49	39	0.5
Lu	0.43	0.61	0.5	0.6	0.13	0.79	0.42	0.36	0.36	0.57	0.18	0.49	0.81	0.83	0.34	0.02
Nd	22.5	26	16.5	20	25.5	24	12	17.5	9	31.5	49	15	29.5	44	29.5	0.02
Pr	7	7	4.1	4.9	8	5.5	2.9	4.7	2	9	15.5	3.6	8.5	13	8.5	0.05
Sm	5	7	4.6	5.5	4.5	7	3.6	4.2	2.8	7	8.5	4.4	7	10	6	0.02
Tb	0.82	1.2	0.85	1	0.48	1.35	0.7	0.67	0.58	1.05	0.81	0.83	1.2	1.6	0.8	0.02
Th	22	7.5	3.5	2.6	29	5.5	1.75	6.5	1.4	15.5	30.5	2.8	24.5	25.5	19	0.02
Tm	0.45	0.65	0.5	0.6	0.15	0.8	0.45	0.4	0.35	0.6	0.2	0.5	0.85	0.9	0.35	0.05
Y	30	42.5	34.5	40	11	54	27.5	26.5	25	41	18.5	34.5	54	60	25.5	0.05
Yb	3.2	4.4	3.5	4.2	0.85	5.5	3	2.5	2.6	4	1.25	3.5	6	6	2.4	0.05

All rare-earth elements expressed as ppm. G = granite, Mix = heterogenous mixing of felsic & mafic, Mp = plagioclase phyric mafic, Mc = coarse grained mafic, Mf = fine grained mafic, Mig = migmatite

Table 5 Representative mineral composition used for P-T estimates on samples from the Harts Range

Mineral:	plag	cpx	opx	ilm	bi	ol	hbd	bi	opx	ilm	plag	cpx	hbd	plag	ilm	hbd	opx	cpx	hbd	hbd
Sample	CL-100	CL-100	CL-100	CL-100	CL-100	CL-100	CL-100	CL-35	CL-35	CL-35	CL-35	CL-35	CL-35	CL-75	CL-75	CL-75	CL-75	CL-75	HR2004-4c	HR2003-14
Rock type	mafic	mafic	mafic	mafic	mafic	mafic	mafic	mafic	mafic	mafic	mafic	mafic	mafic	mafic	mafic	mafic	mafic	mafic	migmatite	granite
SiO2	56.77	54.92	52.77	0.06	37.99	53.21	43.31	37.63	52.89	0.06	55.02	54.93	44.98	52.55	0.00	46.80	52.92	53.81	39.83	39.12
TiO2	0.00	0.04	0.08	52.49	5.58	0.03	1.73	5.57	0.06	51.91	0.00	0.15	1.65	0.04	51.14	0.10	0.05	0.15	1.17	1.61
Al2O3	27.64	1.01	0.89	0.00	14.81	0.92	11.43	14.51	1.28	0.00	29.18	1.08	10.56	29.96	0.00	1.27	1.06	1.15	13.90	11.57
Cr2O3	0.04	0.02	0.06	0.02	0.00	0.05	0.06	0.03	0.09	0.15	0.00	0.05	0.05	0.05	0.02	0.17	0.00	0.00	0.01	0.03
Fe2O3	0.00	0.00	0.00	0.00	0.00	0.00	2.51	0.00	0.00	0.00	0.00	0.00	1.83	0.00	0.00	0.00	0.00	0.00	0.00	23.73
FeO	0.01	20.63	25.72	44.12	15.70	26.74	10.49	16.07	25.84	44.17	0.02	8.80	10.22	0.02	42.21	6.71	23.66	7.49	22.04	0
MnO	0.01	0.64	0.80	0.69	0.11	0.79	0.12	0.03	0.65	0.66	0.00	0.36	0.2	0.03	0.66	0.29	0.63	0.27	0.41	5.51
MgO	0.00	19.18	19.87	0.81	13.01	19.46	11.64	12.92	19.15	1.31	0.00	14.22	12.65	0.00	1.48	12.92	20.59	13.98	5.70	11.28
CaO	6.77	4.01	0.22	0.00	0.04	0.27	9.39	0.00	0.61	0.02	7.96	14.39	8.93	9.19	0.03	18.89	0.33	16.01	10.63	1.36
Na2O	5.64	0.11	0.05	0.06	0.05	0.03	1.29	0.09	0.04	0.00	4.83	0.35	1.26	3.81	0.00	0.35	0.01	0.34	1.09	1.92
K2O	0.14	0.00	0.01	0.01	6.07	0.00	1.05	5.98	0.01	0.01	0.09	0.03	0.83	0.11	0.00	0.00	0.03	0.02	1.71	0
Total	97.02	100.56	100.47	98.26	93.36	101.50	93.01	92.83	100.62	98.28	97.11	94.35	93.16	95.76	95.53	87.49	99.29	93.22	96.89	96.13
Oxygens	8.00	6.00	6.00	3.00	11.00	4.00	23.00	11.00	6.00	3.00	8.00	6.00	23	8.00	3.00	23.00	6.00	6.00	23.00	23
Si	2.59	2.03	1.99	0.00	2.84	1.36	6.62	2.83	1.99	0.00	2.52	2.10	6.8	2.45	0.00	7.45	2.00	2.09	6.18	5.89
Ti	0.00	0.00	0.00	1.01	0.31	0.00	0.20	0.32	0.00	0.99	0.00	0.00	0.187	0.00	1.08	0.01	0.00	0.00	0.14	0.18
Cr	0.00	0.00	0.00	0.00	0.00	0.00	0.01	0.00	0.00	0.00	0.00	0.00	0.006	0.00	0.00	0.02	0.00	0.00	2.54	0.00
Al	1.49	0.04	0.04	0.00	1.31	0.03	2.06	1.29	0.06	0.00	1.57	0.05	1.882	1.64	0.00	0.24	0.05	0.05	0.00	2.05
Fe3+	0.00	0.00	0.00	0.00	0.00	0.00	0.29	0.03	0.00	0.01	0.00	0.00	0.209	0.00	0.00	0.89	0.00	0.00	0.46	2.69
Fe2+	0.00	0.64	0.81	0.94	0.98	0.56	1.34	0.98	0.81	0.93	0.00	0.28	1.293	0.00	0.93	0.00	0.75	0.24	2.40	0.00
Mn	0.00	0.02	0.03	0.02	0.01	0.02	0.02	0.00	0.02	0.01	0.00	0.01	0.026	0.00	0.00	0.00	0.00	0.00	0.05	0.70
Mg	0.00	1.16	1.11	0.03	1.45	0.72	2.65	1.45	1.07	0.05	0.00	0.81	2.851	0.00	0.06	3.07	1.16	0.81	1.32	2.53
Ca	0.33	0.16	0.01	0.00	0.00	0.01	1.54	0.00	0.03	0.00	0.39	0.59	1.447	0.46	0.00	3.22	0.01	0.67	1.77	0.22
Na	0.50	0.01	0.00	0.00	0.01	0.00	0.38	0.01	0.00	0.00	0.43	0.03	0.368	0.34	0.00	0.11	0.00	0.03	0.33	0.56
K	0.01	0.00	0.00	0.00	0.58	0.00	0.21	0.57	0.00	0.00	0.01	0.00	0.16	0.01	0.00	0.00	0.00	0.00	0.34	0.00
Sum	4.92	3.95	3.99	2.00	7.49	2.66	15.30	7.49	3.98	2.00	4.91	3.88	15.228	4.90	1.99	15.01	3.98	3.89	15.52	14.83

Note: HR-2003-14 was sampled by Burdett, 2004 & HR-2004-4c was sampled and analysed by Burdett, 2004

Table 6 Representative mineral composition used for P-T estimates on samples from the Harts Range

Mineral:	plag	opx	cpx	hbd	ilm	unknown	plag	gt	ilm	bi	bi	ilm	gt	hbd	plag	gt	plag	hbd	bi	hbd	hbd
Sample	CL-77	CL-77	CL-77	CL-77	CL-77	CL-77	CL-01	CL-01	CL-01	CL-01	CL-106	CL-106	CL-106	CL-106	CL-106	CL-84	CL-84	CL-84	CL-84	CL-84	CL-84
Rock type	mafic	mafic	mafic	mafic	mafic	mafic	granite	granite	granite	granite	migmatite	migmatite	migmatite	migmatite	migmatite	mixing	mixing	mixing	mixing	mixing	mixing
SiO2	54.59	53.13	53.75	44.97	0.0332	9.2973	59.28	38.56	0.00	37.36	34.78	0.05	37.92	40.93	60.93	38.95	59.61	42.98	37.19	43.95	43.85
TiO2	0.03	0.00	0.15	1.921	52.843	53.1199	0.01	0.00	52.39	5.69	4.45	51.62	0.03	2.74	0.00	0.01	0.06	1.78	4.85	1.80	1.84
Al2O3	28.19	0.96	1.22	11.48	0.0003	7.7384	24.51	21.23	0.00	14.69	14.47	0.00	20.51	12.11	24.36	21.13	25.67	12.60	14.87	12.23	11.93
Cr2O3	0.02	0.01	0.00	0.031	0.0002	0.0002	0.00	0.00	0.02	0.00	0.00	0.00	0.01	0.04	0.06	0.01	0.00	0.04	0.01	0.08	0.01
Fe2O3	0.00	0.00	0.00	0	0	0	0.00	0.00	0.00	0.00	0.00	0.00	0.00	0.00	0.00	0.00	0.00	0.00	0.00	0.00	0.00
FeO	0.08	24.33	7.18	11.48	42.425	23.398	0.04	28.71	43.59	21.37	24.46	43.05	25.63	20.39	0.04	25.21	0.03	17.05	19.92	16.30	16.22
MnO	0.00	0.77	0.25	0.191	0.7512	0.5145	0.00	2.08	0.54	0.00	0.24	1.34	3.15	0.32	0.00	2.61	0.01	0.24	0.14	0.35	0.38
MgO	0.01	21.03	14.12	12.99	1.443	0.9636	0.00	3.53	0.34	9.20	7.17	0.04	1.86	6.12	0.02	3.22	0.00	8.44	10.08	9.43	9.31
CaO	8.30	0.30	17.17	9.068	0.0001	0.0225	4.15	3.18	0.02	0.00	0.02	0.00	7.17	8.00	4.87	6.75	5.42	7.82	0.00	7.28	7.59
Na2O	5.13	0.00	0.26	1.575	0.0458	0.2919	7.32	0.00	0.01	0.09	0.01	0.00	0.02	1.60	7.75	0.03	6.92	1.26	0.06	1.39	1.43
K2O	0.09	0.02	0.00	0.773	0.0126	1.4581	0.21	0.00	0.00	5.42	6.25	0.01	0.02	1.37	0.30	0.00	0.17	1.13	6.36	1.01	1.08
Total	96.44	100.55	94.10	94.49	97.55	96.80	95.52	97.30	96.91	93.85	91.86	96.11	96.31	93.61	98.34	97.93	97.90	93.32	93.49	93.81	93.65
Oxygens	8.00	6.00	6.00	23.00	3.00	3.00	8.00	12.00	3.00	11.00	11.00	3.00	12.00	23.00	8.00	12.00	8.00	23.00	11.00	6.00	6.00
Si	2.52	1.98	2.07	6.67	0.00	0.21	2.69	2.99	0.00	2.85	2.77	0.00	3.10	6.47	2.74	3.10	2.69	6.65	2.84	1.76	1.76
Ti	0.00	0.00	0.00	0.21	1.01	0.89	0.00	0.00	0.92	0.33	0.27	1.01	0.00	0.33	0.00	0.00	0.00	0.21	0.28	0.05	0.06
Cr	0.00	0.00	0.00	0.00	0.00	0.00	0.00	0.00	0.00	0.00	0.00	0.00	0.00	0.00	0.00	0.00	0.00	0.00	0.00	0.00	0.00
Al	1.54	0.04	0.06	2.01	0.00	0.20	1.31	1.94	0.00	1.32	1.36	0.00	1.98	2.26	1.29	1.98	1.37	2.30	1.34	0.58	0.56
Fe3+	0.00	0.00	0.00	0.32	0.00	0.00	0.00	1.68	0.77	0.00	0.12	0.00	0.00	0.00	0.00	0.00	0.00	0.08	0.00	0.00	0.00
Fe2+	0.00	0.76	0.23	1.10	0.90	0.44	0.00	0.00	0.00	1.36	1.51	0.94	1.75	2.47	0.00	1.68	0.00	2.13	1.27	0.55	0.54
Mn	0.00	0.02	0.01	0.02	0.02	0.01	0.00	0.23	0.01	0.00	0.02	0.03	0.22	0.04	0.00	0.02	0.00	0.03	0.01	0.01	0.01
Mg	0.00	1.17	0.81	2.87	0.06	0.03	0.28	0.37	0.00	1.05	0.85	0.00	0.23	1.44	0.00	0.38	0.00	1.95	1.15	0.56	0.56
Ca	0.41	0.01	0.71	1.44	0.00	0.00	0.36	0.00	0.00	0.00	0.00	0.00	0.63	1.35	0.24	0.58	0.26	1.30	0.00	0.31	0.33
Na	0.46	0.00	0.02	0.45	0.00	0.01	0.02	0.00	0.00	0.01	0.00	0.00	0.00	0.49	0.68	0.01	0.61	0.38	0.01	0.11	0.11
K	0.01	0.00	0.00	0.15	0.00	0.04	0.00	0.00	0.00	0.53	0.64	0.00	0.00	0.28	0.02	0.00	0.01	0.22	0.62	0.05	0.06
Sum	4.94	4.00	3.91	15.25	1.99	1.83	4.66	7.20	1.70	7.44	7.54	1.99	7.91	15.35	4.96	7.91	4.93	15.25	7.52	3.98	3.99

Table 7. Sm-Nd and Rb-Sr isotope data for the Stanovos Igneous Complex

Sample	Rock Type	Sm (ppm)	Nd (ppm)	$^{147}Sm/^{144}Nd$	$^{143}Nd/^{144}Nd$	εNd(520)	Sr (ppm)	Rb (ppm)	$^{87}Rb/^{86}Sr$	$^{87}Sr/^{86}Sr$
Cl-01	Granite	6.18	27.87	0.1341	0.51212 ± 4	-6.05	110.6	160.6	4.21600	0.74430
CL-99	Granite	6.18	31.35	0.0828	0.51208 ± 3	-5.69	103.0	217.8	6.14700	0.75550
CL-84	Mafic/felsic mixing	5.67	33.72	0.0903	0.51214 ± 3	-3.40	109.3	115.7	3.07005	0.73234
CL-91	Migmatite	7.21	32.08	0.0710	0.51212 ± 4	-6.14	85.5	197.8	6.72808	0.76066
CL-65	Coarse grained mafic	3.91	13.80	0.1313	0.51260 ± 5	1.03	158.1	17.4	0.31842	0.70749
CL-77	Coarse grained mafic	3.16	10.38	0.1623	0.51272 ± 4	2.39	137.1	12.9	0.27219	0.70606

Table 8. laser ablation - inductively coupled mass spectrometer U-Th-Pb data for zircons from the Harts Range

Spot no.	Description							
sample CL-99	**granite**	**206Pb/238U**	**207Pb/235U**	**207Pb/206Pb**	**Pb206/U238**	**1 sigma**	**Pb207/U235**	**1 sigma**
cl4		0.08211 ± 85	0.66855 ± 761	0.05905 ± 67	508.7	5.04	519.8	4.63
cl7		0.08043 ± 86	0.63714 ± 871	0.05745 ± 8	498.7	5.1	500.5	5.4
cl8		0.08222 ± 86	0.66617 ± 821	0.05876 ± 73	509.4	5.12	518.4	5
cl9		0.08483 ± 89	0.67236 ± 853	0.05749 ± 74	524.9	5.3	522.1	5.18
cl17		0.08482 ± 87	0.67182 ±738	0.05745 ± 63	524.8	5.18	521.8	4.48
cl18		0.08335 ± 89	0.66928 ± 919	0.05824 ± 81	516.1	5.32	520.3	5.59
cl19		0.08008 ± 83	0.63704 ± 739	0.05769 ± 67	496.6	4.98	500.5	4.59
cl20		0.0816 ± 85	0.65181 ± 766	0.05794 ± 68	505.7	5.08	509.6	4.71
cl12		0.08486 ± 88	0.66962 ± 769	0.05723 ± 65	525.1	5.25	520.5	4.68
PSI17 3		0.08352 ± 0.001	0.67047 ± 922	0.05824 ± 73	521	5.61	517.1	5.98
PSI 17 10		0.07968 ± 96	0.64986 ± 93	0.05917 ± 79	508.4	5.03	494.2	4.66
PSI31 10		0.07933 ± 92	0.63923 ± 805	0.05846 ± 67	501.8	4.99	492.1	5.49
PSI17 11		0.0792 ± 89	0.63656 ± 739	0.05831± 62	500.2	4.58	491.3	5.29
17-15		0.08155 ± 100	0.64582 ± 963	0.05745 ± 80	505.9	5.94	505.4	5.97
17-21		0.08157 ± 94	0.64985 ± 837	0.05779 ± 69	508.4	5.15	505.5	5.63
17-28		0.08383 ± 98	0.66331 ± 852	0.0574 ± 67	516.6	5.2	518.9	5.84
17-30		0.08333 ± 96	0.65895 ± 816	0.05736 ± 64	514	4.99	516	5.73
17-32		0.07913 ± 94	0.63801 ± 836	0.05849 ± 70	501.1	5.18	490.9	5.59
17-35		0.08168 ± 100	0.65563 ± 950	0.05823 ± 78	511.9	5.82	506.1	5.95
17-36		0.08285 ± 94	0.65837 ± 784	0.05764 ± 63	513.6	4.8	513.1	5.58
17-50		0.08187 ± 94	0.66648 ± 856	0.05905 ± 70	518.6	5.22	507.3	5.62
17-60		0.08081 ± 97	0.65834 ± 895	0.05909 ± 74	513.6	5.48	501	5.76
17-82		0.08323 ± 101	0.66471 ± 888	0.05793 ± 68	517.5	5.41	515.4	6.03
17-83		0.08307 ± 96	0.65993 ± 820	0.05762 ± 65	514.6	5.01	514.4	5.69
17-84		0.0812 ± 95	0.64515 ± 913	0.05762 ± 77	505.5	5.63	503.3	5.69
17-91		0.08219 ± 99	0.65407 ± 858	0.05771 ± 67	511	5.27	509.2	5.9
Sample CL-01	**granite**							
CL1-3		0.07721 ± 82	0.61688 ± 701	0.05724 ± 62	517.7	4.89	514.2	4.29
CL1-4		0.08362 ± 88	0.65932 ± 787	0.05896 ± 65	553	5.22	555	4.63
CL1-6		0.08956 ± 89	0.72742 ± 763	0.05817 ± 63	555.5	5.24	551.3	4.5
CL1-16		0.08999 ± 84	0.72107 ± 812	0.057 ± 7	513.5	4.98	509.3	4.99
CL1-17		0.08292 ± 90	0.65141 ± 774	0.05877 ± 63	553.7	5.3	554.5	4.55
CL1-20		0.08969 ± 90	0.72647 ± 825	0.05855 ± 68	548.7	5.31	548.9	4.88
CL1-23		0.08885 ± 85	0.71704 ± 769	0.05842 ± 66	521.9	5.07	526.2	4.65

Sample CL-01	**granite (continued)**						
CL1-42	0.08433 ± 75	0.67911 ± 721	0.05803 ± 70	479.4	4.52	487.9	4.53
U3	0.08786 ± 95	0.70127 ± 801	0.05788 ± 63	539.6	5.64	542.8	4.78
D	0.08105 ± 96	0.64462 ± 894	0.05768 ± 75	505.2	5.72	502.4	5.52
H	0.0827 ± 9	0.65543 ± 814	0.05747 ± 68	511.8	5.44	512.2	5
i1	0.0813 ± 93	0.65148 ± 788	0.05811 ± 64	509.4	5.52	503.9	4.85
L1	0.0816 ± 9	0.64927 ± 720	0.0577 ± 60	508	5.25	505.7	4.43
N1	0.08236 ± 95	0.65523 ± 851	0.05769 ± 70	511.7	5.65	510.2	5.22
V1	0.08239 ± 93	0.65622 ± 808	0.05777 ± 66	512.3	5.54	510.4	4.95
X1	0.08069 ± 91	0.64293 ± 765	0.05778 ± 63	504.1	5.43	500.3	4.73
O2	0.0823 ± 10	0.65555 ± 881	0.05777 ±	511.9	5.88	509.8	5.4
K2	0.08237 ± 101	0.66119 ± 900	0.05821 ± 71	515.3	6	510.3	5.5
PP2	0.08501 ± 101	0.67634 ± 872	0.05771 ± 67	524.6	5.98	526	5.28
PP3	0.08285 ± 106	0.66177 ± 1028	0.05793 ± 82	515.7	6.31	513.1	6.28
PP8	0.08267 ± 102	0.66224 ± 878	0.05811 ± 67	516	6.09	512	5.37
Sample CL-106	**Migmatite**						
106-49	0.07969 ± 93	0.63312 ± 902	0.05764 ± 78	494.3	5.04	498	5.21
106-47	0.07892 ± 98	0.61841 ± 90	0.05686 ± 75	489.7	5.13	488.8	4.98
106-43	0.07756 ± 96	0.61729 ± 866	0.05775 ± 72	481.5	5.49	488.1	5.07
106-12	0.07717 ± 94	0.61425 ± 851	0.05774 ± 72	479.2	4.73	486.2	6.01
106-17	0.07757 ± 94	0.62107 ± 835	0.05808 ± 70	481.6	5.03	490.5	5.05
106-18	0.07917 ± 102	0.63133 ± 973	0.05785 ± 80	491.2	5.55	496.9	5.01
106-4	0.07491 ± 97	0.59743 ± 913	0.05786 ± 79	465.7	6.2	475.6	5.07
106-2	0.07803 ± 98	0.62648 ± 846	0.05824 ± 67	484.3	4.82	493.9	5.22
106-11	0.07724 ± 104	0.60821 ± 1022	0.05712 ± 87	479.6	5.97	482.4	5.42
106-36	0.07374 ± 94	0.59018 ± 822	0.05805 ± 70	458.7	5.01	471	4.44
106-10	0.07586 ± 97	0.60718 ± 848	0.05806 ± 70	471.4	5.34	481.8	5.03
106-8	0.07672 ± 101	0.61059 ± 887	0.05773 ± 71	476.5	5.22	483.9	5.1
106-6	0.07944 ± 108	0.63034 ± 1045	0.05756 ± 85	492.8	4.99	496.3	5.46
106-32	0.08156 ± 107	0.64346 ± 951	0.05722 ± 73	505.5	5.67	504.4	6.22
106-31	0.07778 ± 96	0.61388 ± 820	0.05726 ± 67	482.8	5.24	486	4.83
106-16	0.0799 ± 10	0.64436 ± 893	0.0585 ± 7	495.5	5.09	505	5.88
106-52	0.07937 ± 101	0.63712 ± 891	0.05823 ± 70	492.3	5.12	500.5	5.33
106-19	0.07677 ± 90	0.61695 ± 780	0.05829 ± 66	476.8	6.01	487.9	5.07
106-60	0.08206 ± 103	0.65083 ± 917	0.05753 ± 72	508.4	5.8	509	4.77
106-39	0.08096 ± 110	0.65252 ± 1018	0.05846 ± 78	499.7	4.67	517.6	5.08
106-59	0.07825 ± 98	0.62912 ± 872	0.05832 ± 71	485.7	4.87	495.5	5.23

Appendix 1

Beta factor

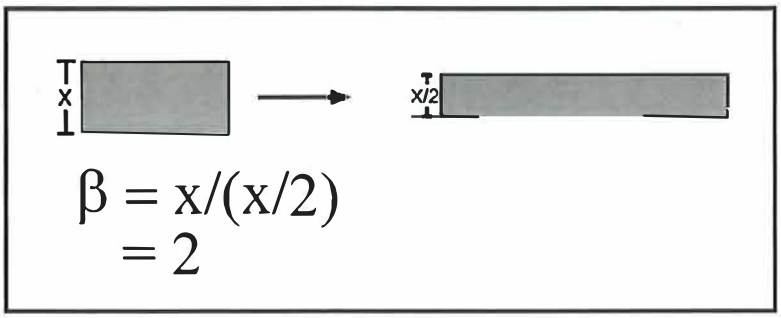

Al-in-hornblende barometer

P = -3.46 + 4.23 * Al

Appendix 2

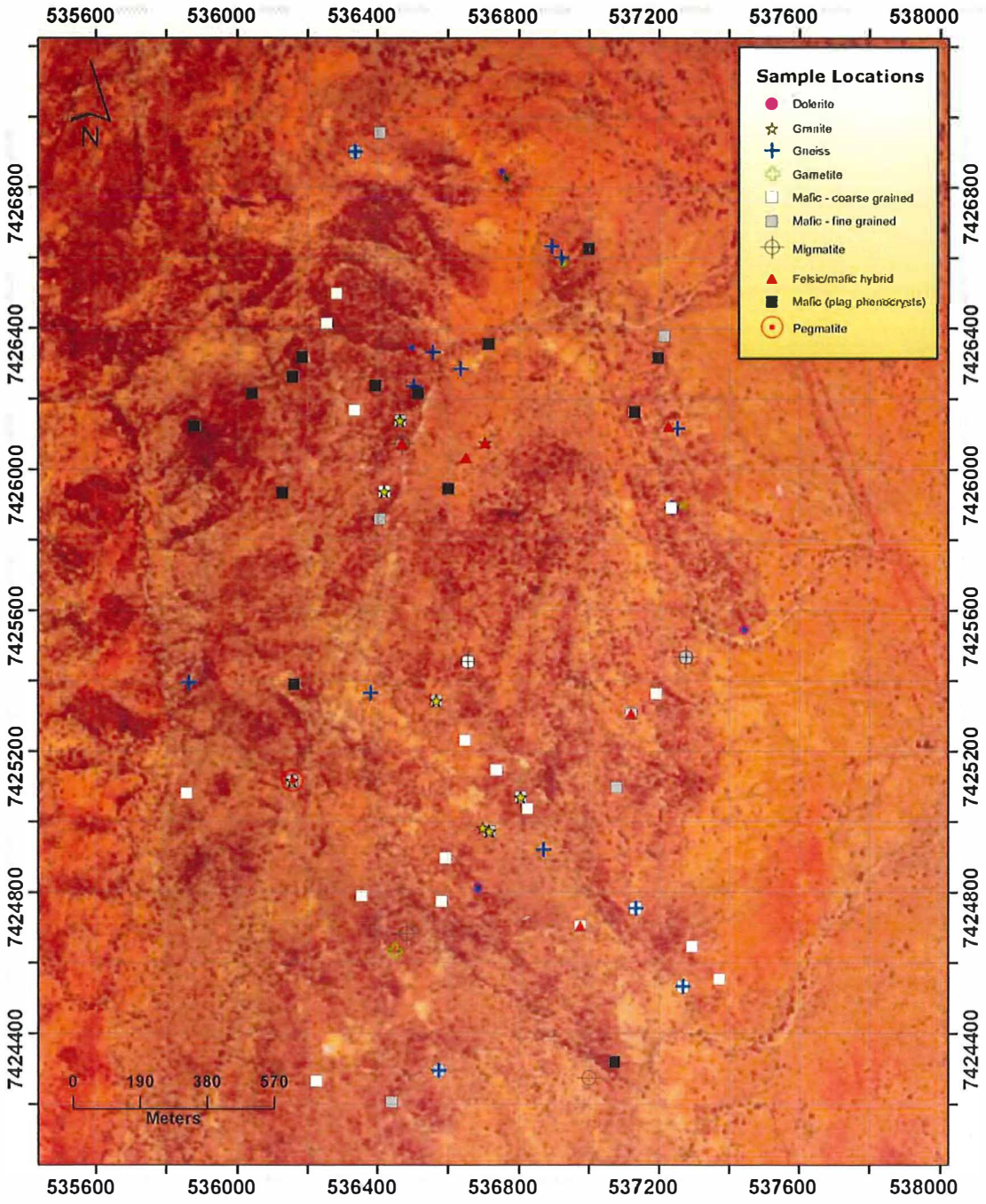

Localities of 122 rock samples collected from the Stanovos Igneous Suite.

Appendix 3.

WGS 84 (Datum) UTM UPS (Coords)

Sample	Eastings	Northings
CL-O1	536699	7424982
CL-O2	536699	7424982
CL-O3	536699	7424982
CL-O4	536699	7424982
CL-O5	536699	7424982
CL-O6	536699	7424982
CL-O7	536699	7424982
CL-O8	536869	7424920
CL-O9	536869	7424920
CL-O10	536920	7426601
CL-O11	536920	7426601
CL-O12	536920	7426601
CL-O13	536920	7426601
CL-O14	536920	7426601
CL-O15	536999	7426628
CL-O16	536999	7426628
CL-O17	536892	7426633
CL-O18	536892	7426633
CL-O19	536892	7426633
CL-O20	536556	7426333
CL-O21	536556	7426333
CL-O22	536556	7426333
CL-O23	536556	7426333
CL-O24	536556	7426333
CL-O25	536556	7426333
CL-O26	536556	7426333
CL-O27	536556	7426333
CL-O28	536556	7426333
CL-O29	536556	7426333
CL-O30	536556	7426333
CL-O31	536514	7426216
CL-O32	536514	7426216
CL-O33	536514	7426216
CL-O34	536514	7426216
CL-O35	536419	7425937
CL-O36	536419	7425937
CL-O37	536601	7425945
CL-O38	536601	7425945
CL-O39	536601	7425945
CL-O40	536601	7425945
CL-O41	536601	7425945
CL-O42	536601	7425945
CL-O43	537268	7424532
CL-O44	537268	7424532
CL-O45	536975	7424703
CL-O46	536975	7424703
CL-O47	536804	7425069
CL-O48	536804	7425069
CL-O49	536648	7425230
CL-O50	536825	7425036
CL-O51	536825	7425036
CL-O52	536736	7425146
CL-O53	536705	7426076
CL-O54	536705	7426076
CL-O55	536651	7426033
CL-O56	536705	7426076
CL-O57	536705	7426076
CL-058(a)	536265	7428472
CL-O58(b)	537214	7426379
CL-O59	537196	7426317
CL-O60	537130	7426163
CL-O61	537252	7426116
CL-O62	537227	7426122
CL-O63	537234	7425891
CL-O64	537234	7425891
CL-O65	536254	7426414
CL-O66	536184	7426319
CL-O67	536333	7426168
CL-O68	536393	7426238
CL-O69	536635	7426285
CL-O70	536714	7426356
CL-O71	536282	7426500
CL-O72	536041	7426216
Cl-073(a)	536405	7426956
CL-O73(b)	536717	7424972
CL-O74	536717	7424972
CL-O75	536593	7424896
CL-O76	536593	7424896
CL-O77	536593	7424896
CL-O78	536448	7424631
CL-O79	536225	7424264
CL-O80	533424	7440258
CL-O81	536501	7426236
CL-O82	536463	7426139
CL-O83	536463	7426139
CL-O84	536468	7426072
CL-O85	536468	7426072
CL-O86	536405	7425859
CL-O87	536656	7425453
CL-O88	536656	7425453
CL-O89	536379	7425364
CL-O90	537277	7425466
CL-O91	537277	7425466
CL-O92	537192	7425363
CL-O93	537120	7425306
CL-O94	537120	7425306
CL-O95	537079	7425097
CL-O96	537134	7424753
CL-O97	537134	7424753
CL-O98	536567	7425343
CL-O99	536567	7425343
CL-O100	537373	7424553
CL-O101	537073	7424319
CL-O102	537000	7424272
CL-O103	536573	7424294
CL-O104	536573	7424294
CL-O105	536440	7424205
CL-O106	536482	7424681
CL-O107	536354	7424789
CL-O108	536155	7425116
CL-O109	536155	7425116
CL-O110	536155	7425116
CL-O111	536335	7426901
CL-O112	536335	7426901
CL-O113	536157	7426263
CL-O114	536127	7425934
CL-O115	536161	7425389
CL-O116	535857	7425080
CL-O117	535863	7425394
CL-O118	537295	7424645
CL-O119	536581	7424773
CL-O120	535878	7426123

Appendix 4

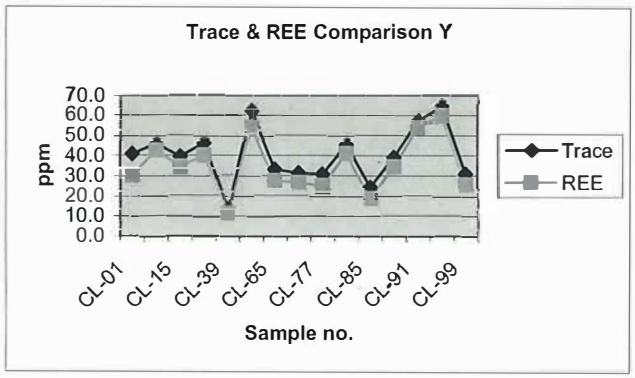
Trace & REE Comparison Y
70.0
60.0
50.0
40.0
30.0
20.0
10.0
0.0
ppm
CL-01
CL-15
CL-39
CL-65
CL-77
CL-85
CL-91
CL-99
Sample no.
Trace
REE

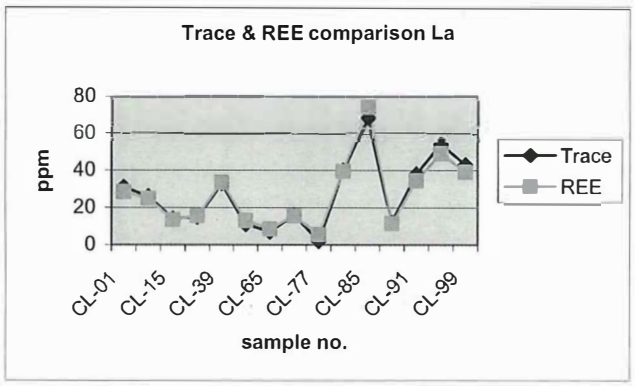
Trace & REE comparison La
80
60
40
20
0
ppm
CL-01
CL-15
CL-39
CL-65
CL-77
CL-85
CL-91
CL-99
sample no.
Trace
REE

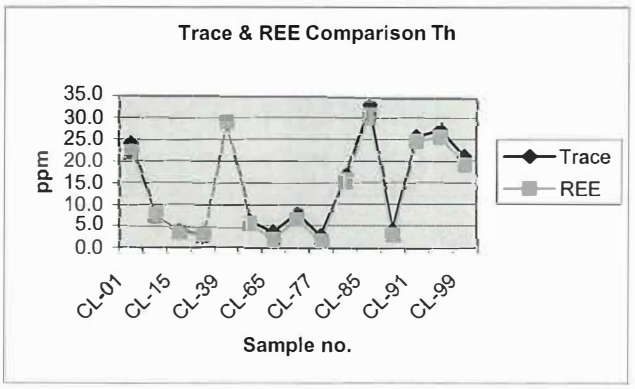
Trace & REE Comparison Th
35.0
30.0
25.0
20.0
15.0
10.0
5.0
0.0
ppm
CL-01
CL-15
CL-39
CL-65
CL-77
CL-85
CL-91
CL-99
Sample no.
Trace
REE

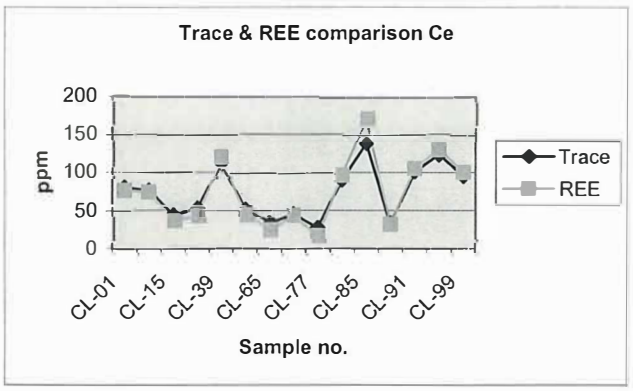
Trace & REE comparison Ce
200
150
100
50
0
ppm
CL-01
CL-15
CL-39
CL-65
CL-77
CL-85
CL-91
CL-99
Sample no.
Trace
REE